Process Safety and Environmental Protection 190 (2024) 298–315

Contents lists available at ScienceDirect

Process Safety and Environmental Protection

journal homepage: www.journals.elsevier.com/process-safety-and-environmental-protection

Transforming a mixture of real post-consumer plastic waste into activated carbon for biogas upgrading

Rafael R. Solís [1], Mónica Calero [*,1], Ledicia Pereira [1], Sandra Ramírez [1], Gabriel Blázquez [1], María Ángeles Martín-Lara [*,1]

Department of Chemical Engineering, University of Granada, Granada 18071, Spain

ARTICLE INFO

Keywords:
Plastic waste
Char pyrolysis
Chemical activation
CO_2 adsorption
Biogas upgrading

ABSTRACT

Plastic waste management is a current environmental issue that demands potential solutions since complete mechanical recycling is limited to the complexity and feasibility regarding the quality and purity of plastic waste. Pyrolysis has emerged as a reasonable solution for the recycling of those fractions that are not further suitable for recycling. Although the implementation of this technology is mature, the generated solid fraction or char has not been completely inserted in the closed loop of plastic recycling. This work explores the possibility of using the carbonaceous char as a precursor for the preparation of porous activated carbons for environmental application as CO_2 adsorbent and biogas upgrading. The effect of the pyrolysis temperature (450 or 500 ºC) on the obtained chars has been assessed for the benefits in the second stage of chemical activation, exploring the possibility of the use of diverse chemical agents. The composition, textural, and surface properties of the porous materials were characterized. N_2 isotherms showed that the char prepared at 500 ºC provided the best textural properties with a performance of $K_2CO_3 \sim KOH > Na_2CO_3 > NaOH > ZnCl_2 > FeCl_3$. Isotherms of CO_2 adsorption showed that the activation with K_2CO_3 displayed the best uptake (130.2 mg g^{-1} at 273 K), closely followed by KOH (125.0 mg g^{-1} at 273 K), also confirmed by dynamic tests in a fixed bed column configuration. The uptake was well correlated with the ultramicropore volume and the oxygenated functional groups. The CO_2 and CH_4 adsorption were studied either in static or dynamic assays. The behavior of the sample activated with K_2CO_3 was studied in detail in column tests, suggesting that the activated material exhibits promising behavior for biogas upgrading.

1. Introduction

In recent years, the identification and evaluation of carbon-based materials have received great attention (Gopinath et al., 2021). Of particular interest are adsorbents derived from low-cost precursors or waste materials, such as those found in large quantities in nature or obtained as a by-product from another industry (Gayathiri et al., 2022). Researchers have proposed a great number of low-cost materials, including date stones (Abbas and Ahmed, 2016; Alhamed, 2009), neem biowaste (Ahmed et al., 2018) rice husk (Alvarez et al., 2015), pineapple plant leaves (Beltrame et al., 2018), sludge (Bian et al., 2018), sugarcane bagasse (Eslami et al., 2018), walnut shell (Li et al., 2018), pistachio shell (Niksiar and Nasernejad, 2017), between others, to remove a wide spectrum of organic and inorganic contaminants from aqueous solutions and gaseous effluents.

Even though plastics are extremely important materials for modern society, despite corporate promises, and international, national, or local governmental responses, plastics production and waste generation continue to rise with deteriorating environmental implications. To reduce environmental impacts throughout the value chain, there is an urgent need to make the lifecycle of plastics more circular.

Pyrolysis is an emerging recycling technology that allows the breaking down of waste plastics into valuable secondary raw materials, including oil, char, and gas (Shah et al., 2023; Wijesekara et al., 2021). Oil can be used as a starting point to produce new chemicals or polymers, and gas is usually used as a versatile energy source that can supply the energetic cost of the process itself. However, during the past decades, little attention has been paid to char products (Ligero et al., 2023b). Pyrolysis addresses environmental issues such as waste management and reducing greenhouse gas emissions. Scaling up pyrolysis

* Corresponding authors.
E-mail addresses: rafarsolis@ugr.es (R.R. Solís), mcaleroh@ugr.es (M. Calero), lpereira@ugr.es (L. Pereira), kazandra1989@gmail.com (S. Ramírez), gblazque@ugr.es (G. Blázquez), marianml@ugr.es (M.Á. Martín-Lara).
[1] Chemical Engineering Department. Faculty of Sciences. University of Granada, Avda. Fuentenueva, s/n 18071 Granada (Spain)

https://doi.org/10.1016/j.psep.2024.07.022
Received 6 February 2024; Received in revised form 4 July 2024; Accepted 6 July 2024
Available online 11 July 2024

treatment can create new revenue streams from the sale of char and oil while reducing reliance on fossil fuels. Economic benefits include job creation, cost savings, generation of renewable energy sources, and potential cost savings through waste management and resource recovery. Environmental benefits include reducing greenhouse gas emissions through char production, converting waste materials into valuable resources, and promoting circular economy principles (Ning et al., 2013; Roy and Dias, 2017).

Plastic-based activated carbons are carbonaceous materials prepared from plastic waste that have been subjected to an activation process to improve their surface area and porosity to raise the capacity to adsorb different types of compounds (Pérez-Huertas et al., 2023). These materials are highly versatile and can be designed to specifically target and remove pollutants, mainly from air and water-polluted effluents (Soffian et al., 2022). Plastic-based activated carbons offer a cost-effective and efficient solution for plastic pollution, especially for plastic waste that cannot be mechanically recycled, closing up the plastic loop (Ligero et al., 2023b).

Diverse activated carbons have already been successfully prepared from plastic-based wastes and implemented to remove diverse contaminants, such as heavy metals (Feng et al., 2018; Mendoza-Carrasco et al., 2016), contaminants of emerging concern (Gómez-Serrano et al., 2021), or polynuclear aromatic hydrocarbons (Ilyas et al., 2021), thus reducing the risk of water contamination and preventing from detrimental effects on ecosystems. Additionally, the use of plastic-based activated carbons in the adsorption of CO_2 from gas effluents has shown promising results, either for the CO_2 capture from combustion effluents (Solís et al., 2023), hence reducing the CO_2 emissions, or offering a potential solution to upgrade biogas into biomethane. A complete review of the use of plastic precursors for the preparation of activated carbons and their evaluation in CO_2 capture has been recently published (Pérez-Huertas et al., 2023). One of the most studied plastic wastes to produce plastic-based activated carbons and its evaluation for CO_2 adsorption is polyethylene terephthalate (PET) (Esfandiari et al., 2012; Kaur et al., 2019b, 2019a; Li et al., 2023; Wang et al., 2020; Yuan et al., 2020), due to its abundant availability and high carbon content (Parra et al., 2004). The PET-derived activated carbons have been demonstrated to perform excellent CO_2 adsorption capacity. For instance, the activation of PET from plastic bottles with KOH at 700 ºC has reported a CO_2 uptake of 4.42 mol kg^{-1} (Yuan et al., 2020), obtained from the isotherms under static analysis. In a similar study, the CO_2 uptake of PET activated with KOH at 700 ºC was 2.31 mol kg^{-1}, obtained in thermobalance analysis (Kaur et al., 2019b). However, PET has not been the only plastic waste used in the development of plastic-based activated carbons for CO_2 capture. Polystyrene (PS) spheres have also been activated, with a previous hydrothermal step, with $ZnCl_2$ leading to a material able to adsorb 3.62 mol CO_2 kg^{-1} (Toprak and Hazer, 2023). Polyurethane was also studied using KOH as a chemical activation agent, obtaining an adsorption capacity of 4.33 mol CO_2 kg^{-1} at 25 °C (Ge et al., 2016). Polyacrylonitrile was also used as a precursor for the preparation of activated carbons that have shown to be good CO_2 adsorbents, reporting adsorption values of 2.5 mol CO_2 kg^{-1}, after activation with KOH at 800 °C for 2 h (Singh et al., 2019). Also, recently, the rejected post-consumer plastic fraction of recycling plants, composed of a mixture of plastics representative of their occurrence in real wastes, have been used as the precursor of the char that was further activated, leading to moderate results of CO_2 adsorption, i.e. 1.11 mol kg^{-1} under KOH activation at 780 ºC (Ligero et al., 2023). However, research using a real mixture of post-consumer plastic polymers in the preparation of activated carbons and their application remains quite limited. In addition, to our knowledge, no studies have investigated the effect of carbonization temperature on the properties and adsorption capacity of plastic-based activated carbons obtained from mixtures of post-consumer plastics.

In this context, with the purpose to help to advance the state of knowledge, this work aims at the development of novel plastic-based activated carbons from a real mixture of post-consumer plastics, collected from the rejected fraction of a municipal solid waste treatment plant. Diverse chemical activating agents have been applied to activate the char collected after the pyrolysis or carbonization of the plastic mixed precursor. Either the temperature of pyrolysis or the nature of the activating agent have been studied on the development of textural properties, and the CO_2 and CH_4 uptake were obtained under static analysis. The activating method with the best performance was selected for a detailed study of the adsorption of CO_2, CH_4, their mixtures, and a simulated biogas formula in dynamic assays in a fixed-bed column setup.

The biogas upgrading integration with pyrolysis creates a holistic approach to waste management that benefits both the environment and the economy. The process promotes circular economy principles and waste materials conversion into valuable resources.

2. Materials and methods

2.1. Chemicals

All the chemicals used were purchased at Merck® as reagent grade (>99 %) and used without further purification. Ultrapure water (18.2 MΩ cm) was obtained from a Direct-Q®-UV device (Millipore®). The commercial formula of zeolite 13X pellets with a spherical shape on average 2 mm diameter was used for comparison purposes with the prepared material.

2.2. Preparation of the novel plastic-based activated carbons

The mixture of post-consumer plastics was collected from the rejection fraction of a municipal solid waste treatment plant. The mixture analysis led to the following composition (wt%): polypropylene, 55.0 %; high-impact polystyrene, 8.6 %; expanded polystyrene, 10.1 %; and polyethylene film, 27.7 %. The characteristics of the plastic waste feedstock were reported in a previous study (Martín-Lara et al., 2021). The mixture, after being crushed to a size inferior to 1 mm, was submitted to a pyrolysis treatment in a horizontal tubular furnace of Nabertherm, under N_2 supply, flowrate of 50 L h^{-1}. The temperature program set stated with a heating rate of 10 ºC min^{-1} from room temperature to the target pyrolysis temperature, i.e. 450 or 500 ºC, and then hold to this value for 90 min.

The resulting char from the pyrolysis was activated under the action of diverse chemical agents, concretely KOH, NaOH, K_2CO_3, Na_2CO_3, $FeCl_3$, and $ZnCl_2$. The chars were crushed and mixed with the chemical activating agent at a mass ratio of 1:1. The mixture was then placed in the tubular furnace and submitted to the following heating program under N_2 feeding (flowrate, 200 mL min^{-1}): heating from room temperature to 300 ºC (heating rate, 10 ºC min^{-1}), next the temperature was kept at this value for 60 min, further raise to 800 ºC (heating rate, 10 ºC min^{-1}), and holding at this value for 60 min. Both activator amount and activation temperature were chosen in accordance with our previous works (Ligero et al., 2023b; Pereira et al., 2024). Then, the resulting solid after the activation stage was washed with HCl solution 1 M, at a proportion of 20 mL per 1 g of char. Following that, the char was filtered and washed with water until obtaining a neutral pH in the filtrate. Finally, the washed activated material was dried overnight at 120 ºC.

2.3. Characterization of the plastic-based activated carbons

The proximate analysis was conducted using a thermobalance from Perkin Elmer®, model STA 6000. A certain amount of sample was placed in a crucible and subjected to the following temperature program under an N_2 atmosphere (flow rate, 20 mL min^{-1}). Firstly, the sample was kept at 30 ºC for 20 min and then raised to 110 ºC (heating rate, 20 ºC min^{-1}) to be held at 110 ºC for 20 min, obtaining the moisture from the weight loss at this stage. Afterward, the volatiles were obtained by raising the temperature to 850 ºC (heating rate, 20 ºC min^{-1}) and kept at this value

for 20 min. For the determination of the ash content, the feeding gas was changed from N_2 to O_2 (20 mL min^{-1}), holding the temperature at 850 ºC for 20 min.

The elemental analysis was quantified in a Thermo Scientific™ CHNS/O analyzer, model Flash 2000. The combustion of the sample at roughly 1400 ºC led to the release of CO_2, H_2O, NO_x, and SO_2 gases that were separated in a chromatographic column and detected on a thermal conductive detector. The oxygen content was estimated from the difference between the CHNS content and the ashes. The surface chemical composition was analyzed by X-ray Photoelectron Spectroscopy (XPS) in a Kratos AXIS Ultra-DLD device equipped with an X-ray source from Al Kα. All the spectra were corrected to the $C_{1\,s}$ peak of adventitious sp^3 carbon to 284.6 eV. The deconvolution of the peaks was processed with the aid of the software XPSpeak 4.1®, under a Shirley background correction.

The textural properties were obtained by static physisorption in a Sync 200 device from 3 P Instruments©. The samples were previously degassed at 150 ºC under vacuum for 12 h on a Prep J4 unit of 3 P Instruments©. The N_2 adsorption-desorption isotherms were obtained at 77 K, leading to the obtention the total surface area by the BET method (S_{BET}, $m^2\ g^{-1}$), the micropore surface area (S_{MP}, $m^2\ g^{-1}$) by t-plot method, the total pore volume (V_T, $cm^3\ g^{-1}$) from the N_2 uptake at p/p_0~0.99, and the micropore volume (V_{MP}, $cm^3\ g^{-1}$) from the t-plot method. The distribution of micropore size was obtained by carrying out CO_2 adsorption isotherms at 273 K, applying the Horvath–Kawazoe (HK) method (Dombrowski et al., 2001; Gauden et al., 2004).

The morphology of the activated samples was analyzed by Scanning Electron Microscopy (SEM) in a FEI Quanta 400 device (30 kV, 3.5 nm resolution). The morphology and chemical composition were further analyzed by Transmission Electron Microscopy (TEM) in a TALOS F200C G2 device (200 kV, 0.3 nm resolution) coupled to an EDX detector Brucker X-flash 6 T-30.

The disorder degree of carbon and the presence of crystalline impurities was analyzed by X-ray Diffraction (XRD) in a Bruker D8 Discover device equipped with a detector Pilatus3R 100 K-A, working with Cu Kα radiation (λ = 1.5406 Å). The diffractograms were registered between the 2θ ranges of 10–85°.

2.4. Adsorption assays of CO_2 and CH_4 on the plastic-based activated carbon

2.4.1. Static adsorption tests

The adsorption of CO_2 and CH_4 was carried out under static mode in a physisorption device (Sync 200 device from 3 P Instruments©), obtaining the isotherms at 273 and 298 K up to 100 kPa. The gas, either CO_2 or CH_4, uptake (q, mg g^{-1}) was adjusted to the Freundlich model (Freundlich, 1907):

$$q = K_F \quad p^{1/n_F} \tag{1}$$

where p is the equilibrium pressure of the gaseous adsorbate, and the K_F (mg g^{-1} kPa^{-nF}) and n_F stand for, respectively, the Freundlich constant and exponent.

The CO_2/N_2 and CO_2/CH_4 selectivity at 298 K was obtained as a function of the total pressure employing the ideal adsorbed solution theory (IAST), considering the typical composition of a post-combustion effluent as 15:85 (v/v) CO_2:N_2 (Espanani et al., 2016) or a biogas fuel as 40:60 (v/v) CO_2:CH_4 (Y. Li et al., 2019a). Hence, the selectivity CO_2/N_2 or CO_2/CH_4 was calculated as follows (H. Li et al., 2019b; Liao et al., 2015):

$$S_{CO_2/N_2} = \left(\frac{V_{CO_2,}}{V_{N_2}}\right)\left(\frac{p_{N_2}}{p_{CO_2}}\right) \text{or} S_{CO_2/CH_4} = \left(\frac{V_{CO_2}}{V_{CH_4}}\right)\left(\frac{p_{CH_4}}{p_{CO_2}}\right) \tag{2}$$

where V_i stands for the gas uptake (STP $cm^3\ g^{-1}$) and p_i is the partial pressure of the i component in the mixture (p_{N2}/p_{CO2}=0.85/0.15, and p_{CH4}/p_{CO2}=0.60/0.40).

The isosteric heat of adsorption (ΔH_{ads}) of CO_2 and CH_4 were calculated as a function of the gas uptake with the Clausius–Clapeyron equation (He et al., 2021; Nuhnen and Janiak, 2020):

$$\Delta H_{ads} = -R\ln\left(\frac{P_2}{P_1}\right)\frac{T_1T_2}{(T_2 - T_1)} \tag{3}$$

For the application of the equation, two isotherms for each gas were carried out and the fitting parameters of the Freundlich model were applied to predict the pressures (p_1 and p_2) at different coverages uptakes (q) at T_1=273 K and T_2=298 K, leading to the isosteric adsorption calculation.

2.4.2. Dynamic adsorption tests in fixed-bed column

Dynamic adsorption tests of CO_2, CH_4, and their mixtures using N_2 as a gas carrier were conducted in a fixed-bed column, leading to the obtention of the breakthrough curves. The plastic-based activated carbon (1 g) was placed in a thermostatic column, 10 cm height and 1 cm internal diameter equipped with a porous ceramic porous at the base, operating at 30 ºC and atmospheric pressure. Glass balls were inserted in the top of the column to prevent possible dragging of the solid. Different adsorption assays feeding 100 mL min^{-1} of gas stream composed of CO_2/N_2 or CH_4/N_2 mixtures from 20/80–80/20 (v/v) were conducted to define the breakthrough curves. The adsorption of CO_2/CH_4 mixtures was also assessed ranging from 50/50–80/20 (v/v). Furthermore, the adsorption behavior with simulated landfill biogas composed of 55 % (v/v) CH_4, 39 % CO_2, 6 % N_2, and trace amounts of O_2 and H_2S was also determined. The concentration of gases in the gas streams was monitored with an INFRA.sens® AK5 device from Wi.tec-Sensorik, based on non-dispersive infrared (NDIR) analysis in a dual beam to analyze both CO_2 and CH_4. The evolution over time of the concentration of gases at the outlet was used to depict the breakthrough curves. The gas adsorption uptake, either for CO_2 or CH_4, was quantified as the area below the adsorbed gas, which means the 1-C_t/C_{inlet} curve, being C_t and C_{inlet} the concentration of the gas at a certain time and the inlet value respectively. The area was computed from the initial time until the saturation time (t_{sat}), defined as the time in which C_{tsat}/C_{inlet}=0.95 (Wang et al., 2015):

$$q = \frac{\vartheta C_0 \int_0^{t_{sat}} \left(1 - \frac{C_t}{C_0}\right) dt}{m_{AD}} \tag{4}$$

where ϑ means the volumetric flow rate (100 L min^{-1}), C_0 (mol L^{-1}) is the inlet CO_2 or CH_4 concentration, and m_{AD} (g) means the mass of adsorbent loaded in the column.

The removal capacity (R) was calculated as the amount of CO_2 retained in the column concerning the total fed CO_2:

$$R = \frac{q_{CO_2} m_{AC}}{\vartheta C_0 t_{sat}} = \frac{\int_0^{t_{sat}} \left(1 - \frac{C_t}{C_0}\right) dt}{t_{sat}} \tag{5}$$

To assess the performance of the CH_4 upgrading, key parameters were estimated: productivity, CH_4 purity, and CH_4 recovery. The molar yield of CH_4 (Y_{CH4}, mol g^{-1} s^{-1}) with a selected purity level (90 %) was determined from the integration of the molar flowrate profile of CH_4 leaving the gas outlet between the time interval of t_1 to t_2, defined as the time where CH_4 reaches the purity selected as 90 % (Álvarez-Gutiérrez et al., 2016; Durán et al., 2022):

$$Y_{CH4} = \frac{1}{m_{AD}} \frac{1}{t_{cycle}} \int_{t_1}^{t_2} F_{CH_4}(t) dt \tag{6}$$

where $F_{CH4}(t)$ is the molar flow of CH_4 in the outlet stream, and t_{cycle} means the necessary time to reach the inlet conditions. Besides, the CH_4 purity was calculated as the percentage of the CH_4 in the outlet gas as follows:

$$CH_4 purity = \frac{\int_{t_1}^{t_2} F_{CH_4}(t)dt}{\int_{t_1}^{t_2} F_{CH_4}(t)dt + \int_{t_1}^{t_2} F_{CO_2}(t)dt} \quad (7)$$

The CH_4 recovery was estimated as the CH_4 extracted in the raffinate during the interval t_1-t_2 concerning the amount fed during the cycle:

$$CH_4 recovery = \frac{\int_{t_1}^{t_2} F_{CH_4}(t)dt}{\int_{0}^{t_{cycle}} F_{CH_4}(t)dt} \quad (8)$$

The adsorption-desorption cycles of reusing with a CO_2-CH_4 mixture were carried out by swapping the inlet with pure N_2 at the same flow rate, i.e. 100 mL min^{-1}. The desorption cycle was finalized when the monitored CO_2 and CH_4 concentrations were negligible.

3. Results and discussion

The evaluation of the solid yield during the production of the plastic-based activated carbons is a relevant aspect to consider since low values increase production costs. Table 1 shows the solid yield defined as the ratio between the mass of plastic-based activated carbon and the mass of plastic precursor used, both on a dry basis, as a function of carbonization or pyrolysis temperature, and the chemical activating agent used. The solid yield was especially affected by the chemical activating agent. However, low changes were observed with the carbonization temperature. Only a low decrease in solid yield was observed as the temperature was increased. The activation with hydroxides (NaOH and KOH) produced the greatest loss of mass, achieving a yield close to 40 % with KOH and 30 % with NaOH. The use of carbonates instead of hydroxides usually reports a higher activated material yield due to the promoted reactions of hydrolysis, de-polymerization, and polymerization with the carbon precursor, triggered in contrast to the oxidation reaction of hydroxides (Sevilla et al., 2021). KOH exhibits more ability to remove more volatile matter during activation if compared to K_2CO_3 (Ahmed and Theydan, 2012). Similarly, the activation process with chlorides, i.e. $FeCl_3$ and $ZnCl_2$, harvested high production yields, providing solid yield values slightly above 50 %. The higher yield achieved during the activation with chloride salts can be explained based on the much more violent reaction triggered by KOH (Ma, 2017). Additionally, in the case of $ZnCl_2$, it has been claimed that displays an inhibition effect on the volatile matter loss, stabilizing it and eventually increasing the yield in comparison with KOH (Pimentel et al., 2023).

3.1. Characterization of the plastic-based activated carbon

The proximate analysis is shown in Table 1 as a function of carbonization temperature and the chemical activating agent used. In general, high ash and low fixed carbon contents were observed in the samples. Also, after cleaning the char with HCl, the ash content decreased, raising the fixed carbon. The chemical activation led to an increase of the fixed carbon, especially in those chars prepared at the higher carbonization temperature, i.e. 500 °C. The highest content of fixed carbon was achieved under activation with sodium-based salts, i.e. NaOH and Na_2CO_3, reaching values of 55.8 % and 53.7 %, respectively.

Some researchers reported similar results regarding the elemental and proximate analysis of char obtained from plastic waste. For example, the pyrolysis of high-density polyethylene (HDPE) waste at temperatures of 400 °C and 450 °C found that the char contained 42.6 % of C and 3.1 % of H (Jamradloedluk and Lertsatitthanakorn, 2014). Also, the pyrolysis of a real mixture of plastic waste from municipal waste has reported an ash content of the char of 61.4 % and a carbon content of 29.3 %, values in the order of magnitude of those found in the char of the current work (Adrados et al., 2012). In addition, the char from the pyrolysis of polyethylene in other studies has been characterized by a volatile matter content of 55.46 %, a fixed carbon content of 15.2 %, and an ash content of 23.6 % (Saptoadi et al., 2016). Therefore, certain variations that highly depend on the characteristics of the plastic raw material used as a precursor to produce the char can be envisaged.

The textural properties were evaluated by N_2 adsorption-desorption isotherms, leading to the results depicted in Fig. 1 and the data summarized in Table 2. The plastic-based activated carbons showed isotherms of type IV according to the IUPAC classification. On the one hand, the isotherms developed a hysteresis between the adsorption and desorption branches because of capillary condensation, which indicates the existence of mesopores. On the other hand, the marked slope at low relative pressures proves the existence of micropores. The char obtained by pyrolysis at temperatures either 450 °C or 500 °C exhibited very low S_{BET} (below 4 m^2 g^{-1}). After treatment with HCl, a slight increase is observed, probably due to the cleaning effect during the acid treatment, which reduces the ash content and contributes to cleaning some micro, and overall mesopores (Ariyadejwanich et al., 2003). However, an outstanding increase in porosity was accounted for after chemical activation, an essential factor for CO_2 adsorption, in which micropore volume has been claimed as the key parameter to enlarge the CO_2 uptake at mild conditions (Varghese et al., 2023). Little differences in the textural properties were observed after activation of the chars carbonized at 450 °C and 500 °C by each chemical agent. As revealed in Table 2, the porosity order was K_2CO_3 > Na_2CO_3 > KOH > NaOH > $ZnCl_2$ > $FeCl_3$ for those chars pyrolyzed at 450 °C. For the chars pyrolyzed at 500 °C, the effect of KOH overpassed the Na_2CO_3, probably due to the higher

Table 1
Elemental and proximate analyses of the plastic-based activated carbon from chars obtained at 450 and 500 °C.

Material	T* (°C)	Yield (%)	Elemental analysis (wt., %)					Proximate analysis (wt., %)			
			C	H	N	S	O	Moisture	Volatile	Fixed carbon	Ash
Char	450	-	35.4	2.6	1.0	-	21.8	0.9	36.0	23.9	39.2
Char-washed		-	49.3	4.1	1.5	-	14.4	0.7	36.4	32.1	30.8
Char-NaOH		30.0	35.2	0.8	-	-	16.2	5.4	15.4	31.4	47.8
Char-Na_2CO_3		45.2	48.7	0.8	0.9	0.6	17.0	7.7	28.7	31.5	32.1
Char-KOH		40.5	24.8	0.9	0.3	-	16.9	6.5	17.6	18.7	57.2
Char-K_2CO_3		38.5	43.9	0.6	0.8	0.8	11.1	5.4	10.2	41.6	42.9
Char-$FeCl_3$		51.0	45.4	0.6	0.8	0.7	13.2	2.8	8.1	49.8	39.4
Char-$ZnCl_2$		44.5	42.0	0.5	0.9	0.8	11.3	5.9	7.0	42.7	44.5
Char	500	-	37.0	2.4	1.0	-	19.9	2.9	30.0	28.3	38.8
Char-washed		-	52.2	5.1	1.5	-	5.3	1.6	32.0	30.5	35.9
Char-NaOH		29.4	55.0	0.7	0.7	-	12.5	4.8	8.2	55.8	31.2
Char-Na_2CO_3		41.1	55.5	0.8	1.0	-	7.7	2.6	8.8	53.7	35.0
Char-KOH		34.7	49.0	0.5	0.6	-	13.7	7.2	9.3	47.3	36.2
Char-K_2CO_3		40.6	47.6	1.0	0.5	-	12.7	1.7	11.0	49.0	38.3
Char-$FeCl_3$		53.0	49.1	0.5	0.8	0.7	5.2	2.3	7.1	46.9	43.7
Char-$ZnCl_2$		55.0	48.0	0.4	-	0.7	7.4	1.6	5.6	49.3	43.5

* Temperature for the carbonization or pyrolysis of the plastic mixture.

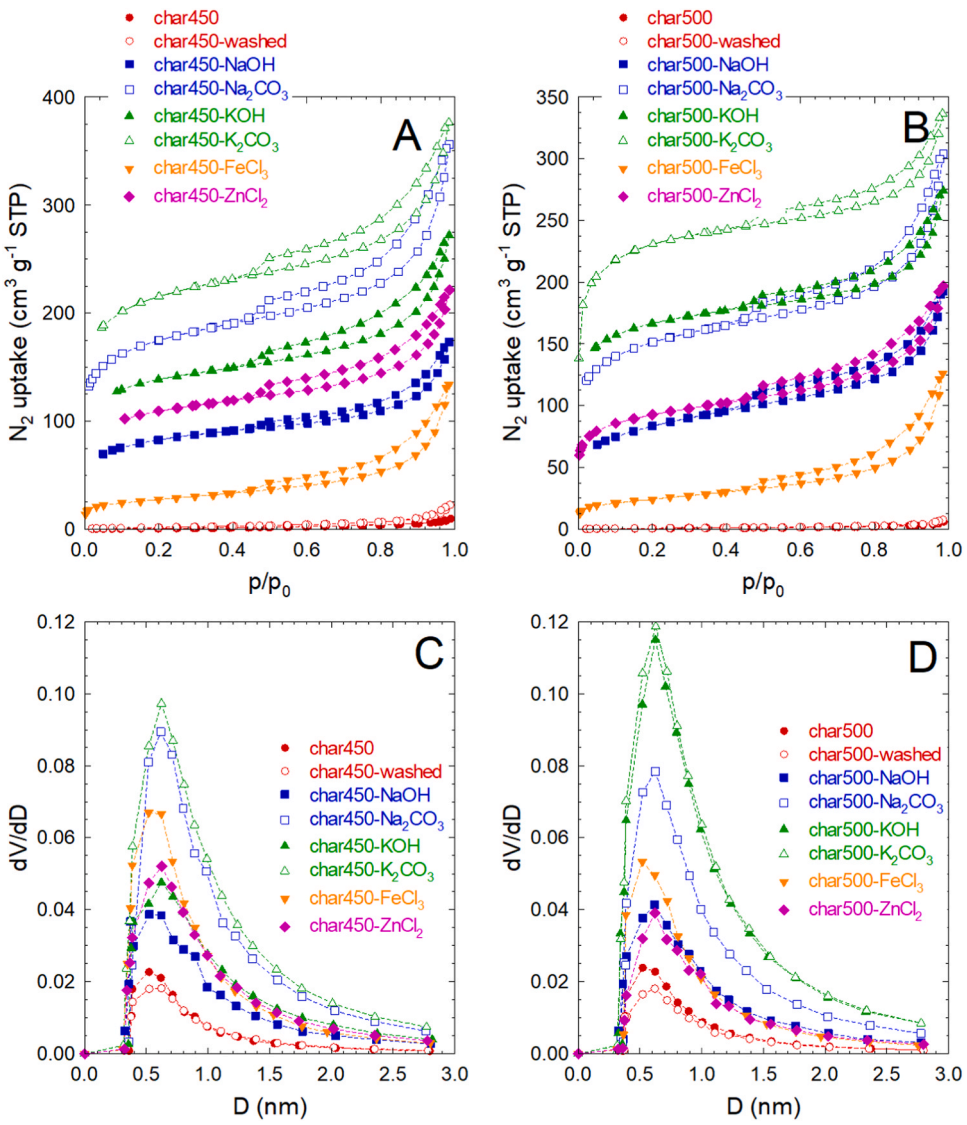

Fig. 1. N_2 adsorption-desorption isotherms of plastic-based activated carbons prepared from carbonized chars at 450 ºC (A) and 500 ºC (B) and their respective pore-size distribution (C and D).

reactivity of KOH if compared to Na_2CO_3. Interestingly, the chars carbonized at 500 ºC led to the highest microporosity, being the uppermost V_{MP}/V_T ratios registered after activation with K_2CO_3 (58,9 %, V_{MP}=0.307 cm^3 g^{-1}) and KOH (50.0 %, V_{MP}= 0.212 cm^3 g^{-1}). The micropore size distribution, depicted in Fig. 1 C-D demonstrates a centered distribution of micropores around 0.7 nm, with a better definition in the chars carbonized at 500 ºC and activated with K_2CO_3 and KOH.

Our findings show that the carbonization temperature exerts a positive effect on the activation process, with better results obtained at 500 °C compared to 450 °C. The reactions in the carbonization process included volatilization, functional group breakage, and aromatic ring polycondensation (Zhang et al., 2024). However, the plastic waste cannot be carbonized completely at low temperatures. If the temperature is too high, some pores are sintered, decreasing the specific surface area and pore volume. For example, it has been reported that the carbonization temperature significantly influenced the specific surface area and pore volume of activated coal char, firstly increasing with the carbonization temperature and then dropping as the carbonization temperature rose (Quan et al., 2021). The activated carbon with the best pore structure was the one that was carbonized at 600 °C. The textural properties of activated coal char were positively correlated with the CO_2 adsorption capacity, with the microporous volume being the primary factor.

If surface areas of developed plastic-based activated carbons in this study are compared with commercial activated carbons, the obtained values are quite low compared to those obtained from biomass. In this case, the composition of plastic plays an important effect. The complex and heterogenous composition of the mixture of plastics used in this work resulted in an activated carbon product with a lower surface area, i.e. 804 m^2/g, than other commercial activated carbons prepared mainly from homogeneous biomass precursors as summarized in Table 3.

Generally, KOH is the most popular chemical activating agent due to its strong basic character to destroy diverse carbon walls, leaving the formation of micropores, even in plastic-based precursors such as PET bottles (Gómez-Serrano et al., 2021; Kaur et al., 2019a; Yuan et al., 2020), PVC (Lian et al., 2011), polystyrene foams (de Paula et al., 2018), and tires (González-González et al., 2020; Teng et al., 2011). However, the porosity generated, strongly depends on the composition of the precursor, among other variables. The development of pores during KOH activation is intrinsically associated with a gasification reaction, which occurs according to the overall reaction provided below.

$$6KOH + 2\,C \rightarrow 2\,K + 3H_2 + 2K_2CO_3$$

Table 2
Textural properties and CO_2 uptake of the plastic-based activated carbons.

Material	T* (ºC)	N_2 isotherm at 77 K						CO_2 uptake at 100 kPa	
		S_{BET} ($m^2\ g^{-1}$)	S_{MP} ($m^2\ g^{-1}$)	V_T ($cm^3\ g^{-1}$)	V_{MP} ($cm^3\ g^{-1}$)	V_{MP}/V_T (%)	D_{MP} (nm)	q_{CO2} at 273 K (mg g^{-1})	q_{CO2} at 298 K (mg g^{-1})
Char	450	3.3	-	0.015	-	-	-	16.8	10.4
Char-washed		7.4	-	0.035	-	-	-	16.8	11.0
Char-NaOH		265.0	178.9	0.268	0.091	34.0	0.70	42.8	29.2
Char-Na_2CO_3		608.9	387.8	0.551	0.200	36.3	0.75	93.5	64.1
Char-KOH		483.1	311.1	0.421	0.163	38.7	0.74	58.6	41.3
Char-K_2CO_3		750.3	545.8	0.583	0.262	44.9	0.75	107.0	67.6
Char-$FeCl_3$		93.3	26.6	0.207	0.013	6.3	0.67	58.4	33.7
Char-$ZnCl_2$		350.2	242.8	0.343	0.123	35.8	0.73	55.0	34.6
Char	500	2.1	-	0.009	-	-	-	20.3	13.6
Char-washed		2.7	-	0.012	-	-	-	17.0	11.2
Char-NaOH		290.8	147.6	0.298	0.074	24.8	0.74	45.3	29.1
Char-Na_2CO_3		529.7	352.1	0.470	0.171	36.4	0.74	84.1	58.3
Char-KOH		580.4	406.3	0.424	0.212	50.0	0.75	125.0	84.8
Char-K_2CO_3		803.7	577.2	0.521	0.307	58.9	0.74	130.2	82.1
Char-$FeCl_3$		83.1	16.8	0.195	0.009	4.6	0.67	47.1	43.5
Char-$ZnCl_2$		288.4	180.0	0.304	0.097	31.9	0.75	38.6	29.8

* Temperature for the carbonization or pyrolysis of the plastic mixture.

Table 3
Comparison of surface area of commercial activated carbons.

Commercial activated carbon	Surface area (m^2/g)	Reference
Norit® SX2 POCH-Poland	659	(Lota et al., 2008)
YP-50 F, Kuraray Chemical Corporation, Japan	1690	(Bang et al., 2017)
Precursor coconut shell, Kuraray Co., Ltd	1700	(Zhang et al., 2022)
Precursor coconut shell, Kuraray Co.,Ltd	2426	
Precursor coconut shell, Fuzhou Yihuan Carbon Co. Ltd.	2429	
Precursor coconut shell, Beike 2D materials Co. Ltd.	1327	
Precursor petroleum coke, XFNANO Co, Ltd	2125	
Precursor petroleum coke, Fuzhou Yihuan Carbon Co. Ltd.	2074	
Precursor petroleum coke, Fuzhou Yihuan Carbon Co. Ltd.	2145	
Precursor not specified	1370	(Otsuki et al., 2007)
Precursor coconut shell	1343	(Sitthikhankaew et al., 2011)

When KOH is added to the carbonized plastic, the formation of K_2CO_3 is expected at around 400℃, leading to a complete transformation of KOH into K_2CO_3 at around 600℃. Later, K_2CO_3 oxidizes the carbonaceous matter to CO yielding porosity in the carbon residue with a maximum release of CO up to 800℃ (Lozano-Castelló et al., 2007; Raymundo-Piñero et al., 2005) according to the following chemical reaction.

$$K_2CO_3 + 2C \rightarrow 2\ K + 3CO$$

The difference between the potassium hydroxide and carbonate relies on the oxidation of the carbon matter, which starts at over 600–700 ºC for K_2CO_3 (Sevilla and Fuertes, 2016), whereas the redox reaction of KOH with the carbon precursor is triggered at lower temperatures (~ 400 ºC) (Lillo-Ródenas et al., 2003). This may explain the controlled reaction of K_2CO_3 versus the most aggressive KOH, leading to better conservation of the micropore morphology by the carbonate (Sevilla et al., 2021). Probably the greater aggressivity of KOH explains the lower microporosity for the plastic-based char if compared to K_2CO_3. In fact, the comparison performance of K_2CO_3 and KOH has been reported a better control the micropore size distribution by K_2CO_3, enhancing the CO_2 capture when used as adsorbent (Wang et al., 2022). Regarding the effect of NaOH or Na_2CO_3, much less researched as an activating agent inf compared to their K salts (Pérez-Huertas et al., 2023), it should be noticed that NaOH is less corrosive than KOH, Na_2CO_3 offers a lower catalytic activity of Na_2CO_3 for carbon gasification and the higher temperature of decomposition into CO_2, e.g. 1000 ºC (Kim and Lee, 2001). Concerning the use of chlorides (neutral activating agents), the main mechanisms for pore formation are oxidation, template, and gasification. $ZnCl_2$ performed better ability to develop micropores whereas the surface created by $FeCl_3$, much lower, was mainly of a mesopore nature. $ZnCl_2$ plays a key role in the removal of hydroxyl groups during activation, enabling the removal of oxygenated groups from the structure, and accelerating the dehydration reaction which releases more porous structures if compared to $FeCl_3$ (Liu et al., 2021).

To investigate the influence of the activating agent on the presence of oxygenated surface groups, XPS was conducted, selecting the char activated at 500 ºC due to the better performance observed of the textural properties. The composition of the surface is summarized in Table 4. The results demonstrate the presence of carbon and oxygen at the surface as major components. The minor detected elements were Si and Ti, among others such as Ca or Fe. The existence of these elements is due to the addition of popular chemical additives to the formulation of

Table 4
Chemical surface composition by XPS of the activated chars at 500 ºC.

Material	Composition (% wt.)				
	C	O	Si	Ti	Others
Char	79.6	13.1	0.6	-	Ca (4.3)
Char-washed	87.2	10.4	1.6	0.9	-
Char-NaOH	51.6	25.2	8.0	4.1	Ca (2.3) Fe (1.8) Na (1.0)
Char-Na_2CO_3	55.1	23.2	5.1	6.7	Ca (1.4) Fe (2.0) Na (1.8)
Char-KOH	50.7	27.5	5.7	6.0	Ca (1.4) Fe (3.7) K (1.0)
Char-K_2CO_3	65.0	29.1	6.3	4.0	Ca (1.2) K (1.7)
Char-$FeCl_3$	80.3	12.3	2.0	1.4	Ca (1.5) Fe (2.1)
Char-$ZnCl_2$	77.4	12.9	4.3	1.5	Zn (3.2)

the plastic, for instance, colorants (TiO_2) lubricants (siloxane), flame-retardants (SiO_2), and fillers ($CaCO_3$ and silicate) (Tang et al., 2023). These minor elements suffered a concentration effect after activation during their accumulation. The activating agent reacts with the carbon content to develop the porosity, leaving them more concentrated in the final material. The activation process positively impacted the release of oxygenated groups, especially with KOH (27.5 %) and K_2CO_3 (29.1 %), followed by their sodium counterparts. However, $FeCl_3$ and $ZnCl_2$ did not exert this effect as the oxygen at the surface was barely 12 %. The lower oxygen content for the carbons activated with $ZnCl_2$ if compared to KOH has been attributed to the catalytic dehydration effect caused by $ZnCl_2$ (Pimentel et al., 2023). The activation of $ZnCl_2$ leads to higher the removal of the hydrogen and oxygen atoms from the activated carbon structure (Heidarinejad et al., 2020). It has been stated that hydroxides and carbonates display a great ability to create highly oxygenated basic groups if compared to acidic metals which tend to develop neutral and faintly acidic groups (Gao et al., 2020; Sevilla et al., 2021).

A qualitative analysis of the oxygenated groups was further assessed in the samples prepared from the chars activated at 500ºC. As an example, the high-resolution spectra for $C_{1\,s}$ and $O_{1\,s}$ of the samples char500-KOH and char500-K_2CO_3, are depicted in Fig. 2. The distribution of the different considered groups is shown in Table 5 for all the samples. Regarding the $C_{1\,s}$ spectrum, the following contributions were considered for the deconvolution: C═C (284.6 eV), C-C (285.3 eV), C-O (286.6 eV), C═O (288.0 eV), and O═C-OR (289.9 eV) (Ramírez-Valencia et al., 2023). In terms of oxygen bonded to surface carbon, it is appreciated that the washing led to an important abatement of the contribution of oxygenated carbon as shown in the result of

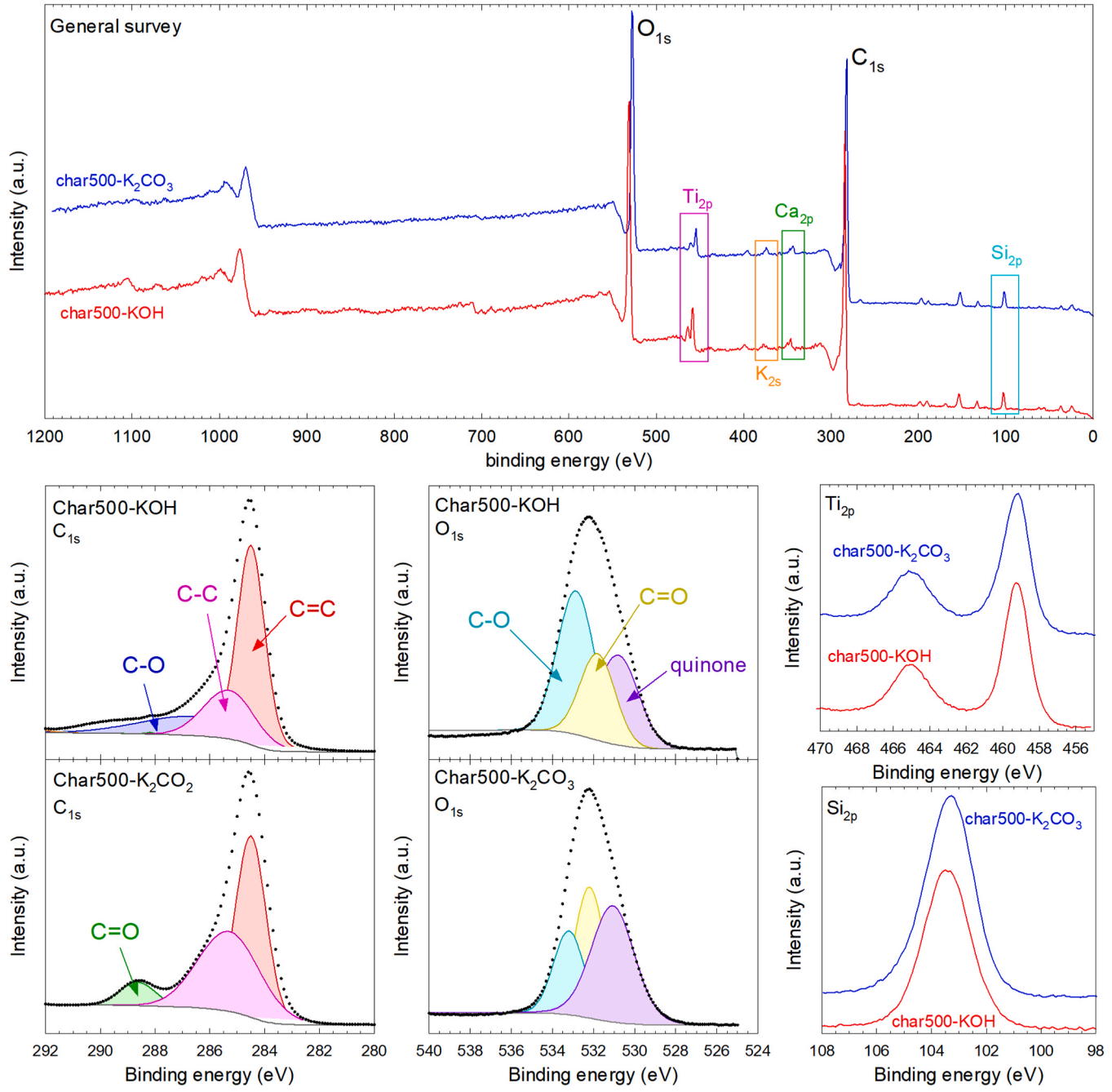

Fig. 2. XPS general survey (top) and high-resolution spectra of the $C_{1\,s}$ (bottom left), $O_{1\,s}$ (bottom middle), Si_{2p}, and Ti_{2p} (bottom right) regions of samples char500-KOH and char500-K_2CO_3.

Table 5
Surface oxygenated composition by XPS of the chars prepared at 500ºC.

Sample	C_{1s}			O_{1s}		
	Type	BE (eV)	% Peak	Type	BE (eV)	% Peak
Char500	C═C	284.4	43.4	quinone	531.3	39.7
	C-C	285.3	27.0	C═O	532.5	33.2
	C-O	286.0	26.3	C-O	533.7	27.1
	C═O	288.5	2.6			
	COO-	290.0	0.7			
Char500-washed	C═C	284.4	51.2	quinone	531.6	38.2
	C-C	285.3	42.6	C═O	532.4	34.0
	C-O	286.7	3.0	C-O	533.6	27.8
	C═O	288.9	3.3			
	COO-	290.0	0.0			
Char500-NaOH	C═C	284.5	45.4	quinone	531.3	24.8
	C-C	285.3	27.1	C═O	533.0	51.0
	C-O	286.5	15.0	C-O	534.3	24.2
	C═O	288.9	1.5			
	COO-	289.4	11.0			
Char500-Na_2CO_3	C═C	284.5	47.4	quinone	531.9	32.7
	C-C	285.3	35.0	C═O	532.5	41.1
	C-O	286.5	13.0	C-O	533.6	26.1
	C═O	289.0	3.5			
	COO-	290.0	1.1			
Char500-KOH	C═C	284.5	52.7	quinone	530.8	30.5
	C-C	285.3	22.4	C═O	531.8	25.3
	C-O	286.6	18.3	C-O	532.8	44.2
	C═O	288.7	0.2			
	COO-	289.9	3.8			
Char500-K_2CO_3	C═C	284.5	48.4	quinone	531.0	44.7
	C-C	285.3	42.1	C═O	532.0	33.0
	C-O	286.6	0.6	C-O	533.2	22.3
	C═O	288.6	7.1			
	COO-	289.9	0			
Char500-$FeCl_3$	C═C	284.5	49.9	quinone	530.6	17.2
	C-C	285.3	37.2	C═O	532.4	50.3
	C-O	286.5	0.0	C-O	533.8	32.5
	C═O	288.5	12.9			
	COO-	290.0	0.0			
Char500-$ZnCl_2$	C═C	284.5	50.8	quinone	531.2	16.7
	C-C	285.3	23.3	C═O	532.5	32.5
	C-O	286.5	17.2	C-O	533.6	50.8
	C═O	289.2	2.1			
	COO-	290.2	6.6			

Table 4 for char before and after washing with HCl. The activation with NaOH and Na_2CO_3 led to the development of C-O groups. The C-O groups are more abundant in char500-KOH while C═O is the more abundant contribution in char500-K_2CO_3. The activation with $FeCl_3$ is enriched with C-O groups while $ZnCl_2$ conducts the formation of C═O. The O_{1s} region was fitted to quinone (530.7 eV), C═O (531.5–532.0 eV), and C-O (~533 eV) (Burg et al., 2002). From the analysis of the O_{1s} region, it is appreciated an outstanding contribution of C═O, attributable to ketones, lactones, acids, esters, and quinonic groups in the char500- K_2CO_3 and char500-$ZnCl_2$. The sample activated with KOH displayed an equilibrated contribution in which a major contribution of C-O (ethers and alcohols) was observed. Finally, regarding the metals at the highest concentration, i.e. Si and Ti, their high-resolution spectra suggested their presence at their highest oxidation estate, which means Si^{4+} and Ti^{4+}. The Si_{2p} spectra in Fig. 2 depict a maximum peak centered at roughly 103.5 eV, a value close to the reported for SiO_2 (Koshizaki et al., 1998). In the case of Ti_{2p}, a peak at 459.1 eV for $Ti_{2p3/2}$ and another at 465.0 eV for $Ti_{2p1/2}$ were recorded. These values suggest the presence of Ti^{4+} as reported in the literature (Biesinger et al., 2010).

The analysis of the disorder degree of carbon and the presence of crystalline impurities was analyzed by XRD. Fig. 3 portrays the diffractograms of the two samples with the best-developed textural properties, i.e. char500-KOH, and char500-K_2CO_3. The disorder degree has been reported in activated carbon with the presence of broadband centered at roughly 24 and 43º, attributed to the (002) and (100) diffraction planes (Bedia et al., 2020), being the response of the small number of stacked layers with uniform interlayer distance associated to the presence of ordered graphite or graphene structures (Li et al., 2007). However, this was not the case for the prepared activated carbon from plastic residue. A considerable important contribution of crystalline phases is depicted, linked to the presence of impurities. The identification of the crystalline pattern concluded the presence of the orthorhombic phase of the perovskite $CaTiO_3$ (COD-9013383). According to XPS analysis, considerable amounts of Ca and Ti were detected on the surface which is consistent with the conclusion reached by XRD.

The morphology of the most porous samples, i.e. char500-KOH and char500-K_2CO_3 was analyzed by SEM microscopy. The SEM micrographs illustrated in Fig. 4 suggest the development of a porous surface after activation using both activation agents. No significant morphological differences were appreciated since the mechanism of both relies on the reaction and decomposition of the chemical agent with the organic content to release CO and CO_2. However, as claimed in the literature (Sevilla et al., 2021), the activation with K_2CO_3 triggers a less aggressive reaction leading to a material that resembles the structure pattern of the carbon precursor. In contrast, KOH has ability of destroying at higher extend the carbon material.

Finally, it is important to specify that the high boiling point of KOH (1327 °C) suggests that some of it remains after the activation process after the acid washing. This leftover KOH may be extremely dangerous to the environment if not disposed of properly. These consequences tend to outweigh the advantages of producing porous carbons using KOH-based chemical activation, and they highlight the need to look for more effective yet environmentally acceptable chemical activation reagents (Singh et al., 2023). In addition, KOH has some limitations concerning its corrosiveness, equipment deterioration, and environmental toxicity (Gao et al., 2020).

Transmission electron microscopy (TEM) images, see Fig. 5, of the activated carbon samples, also offered valuable insights into the structural and morphological characteristics. TEM images of char500 and char500-washed show that the particles are predominantly irregular sheets, typical of carbon materials after thermal activation processes. However, after activation certain destruction of the carbon particles can be envisaged. The presence of wrinkled sheets, pores, and cavities is predominant, reflecting a consistent activation process. Moreover, some TEM images show occasional impurities and inclusions, possibly remnants of additives of plastic precursor materials. The EDS analysis of the sample displayed some regions with crystalline opaque particles of Ca and Ti (Fig. 5 D1), compatible with the $CaTiO_3$ detected by the XRD technique.

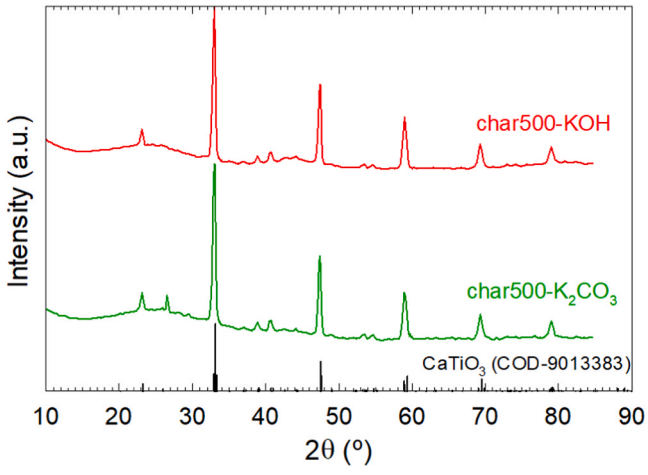

Fig. 3. XRD patterns of the char500 activated with KOH and K_2CO_3.

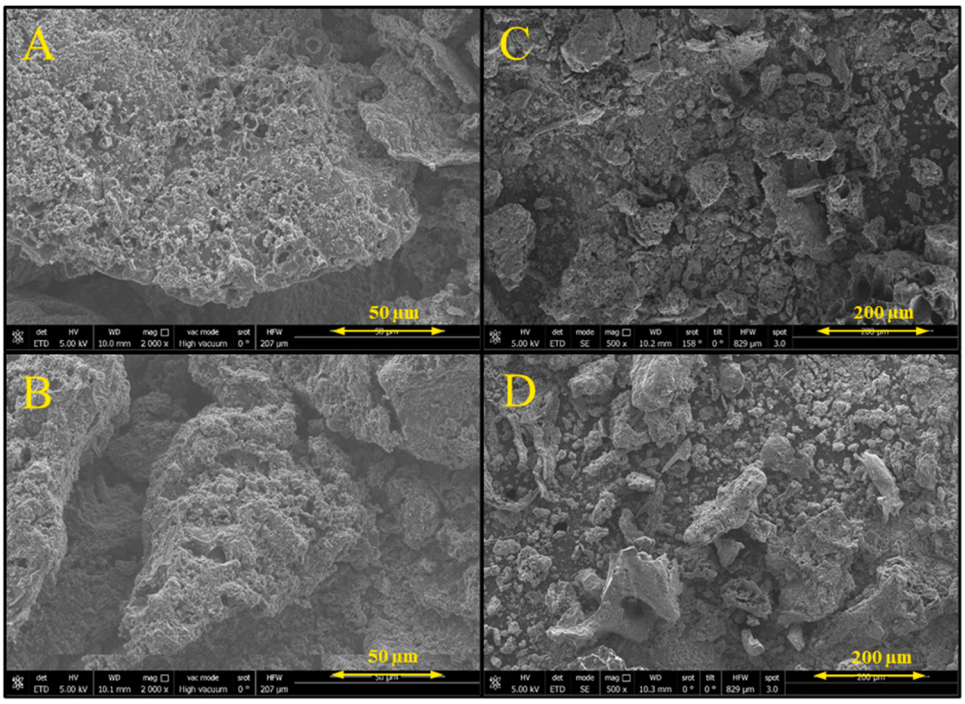

Fig. 4. SEM pictures of the samples char500 (A), char500-washed (B), char500-KOH (C), and char500-K_2CO_3 (D).

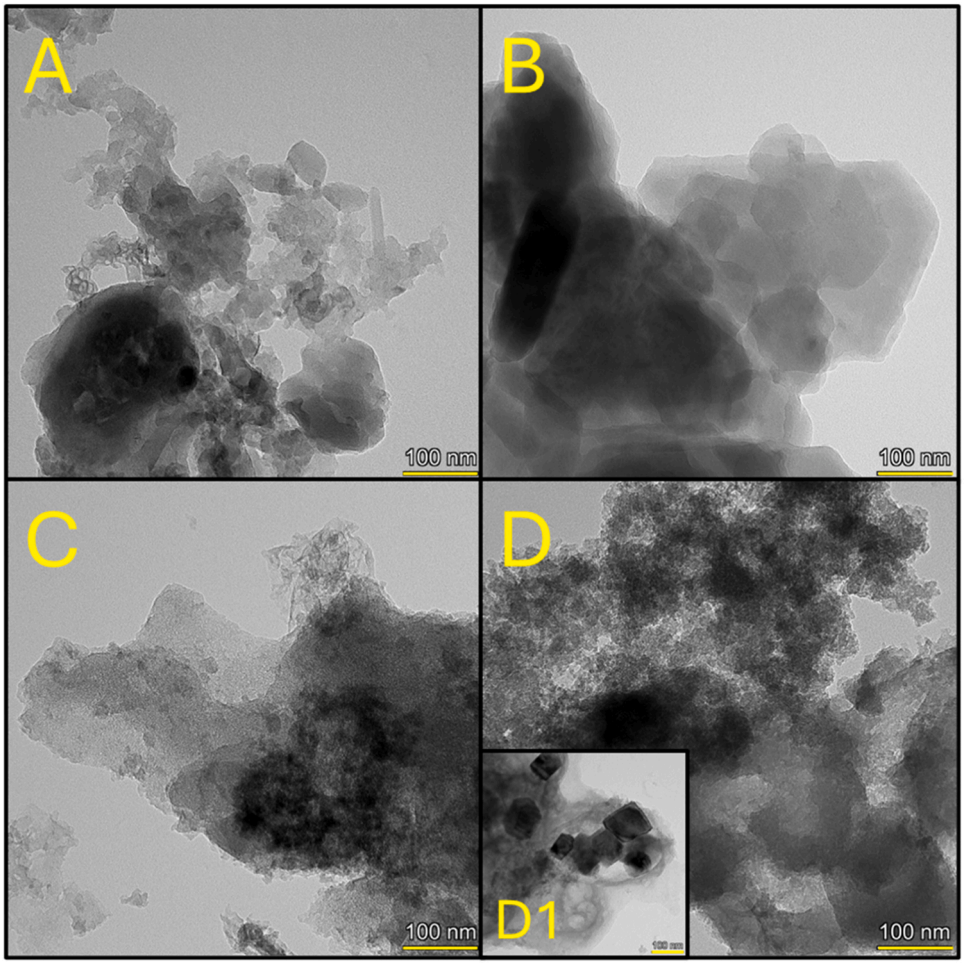

Fig. 5. TEM pictures of the samples char500 (A), char500-washed (B), char500-KOH (C), and char500-K_2CO_3 (D and D1).

3.2. Adsorption capacities of CO_2 and CH_4

Table 2 also summarizes preliminary adsorption uptakes of CO_2 at 100 kPa. It is observed that the native and cleaned char had a low adsorption capacity, slightly increased when the temperature was elevated from 450 to 500 °C. The activated samples, whose CO_2 adsorption capacity is much higher in some activating agents, corroborated that the char prepared at 500 °C displayed better affinity towards CO_2 adsorption, due to better reactivity toward the activating agent and therefore raised the development of micropores. Based on that, the adsorption behavior of CO_2 and CH_4 was detailly assessed in static assays in a physisorption device up to 100 kPa, for those chars carbonized at 500 °C due to the boosted micropore volume in these activated chars.

The CO_2 uptake reported for other plastic-based activated carbon is very variable depending on the origin of the material devoted for the preparation of the char and the method followed for the activation. For example, the activation with KOH and NaOH of PET bottles has reported CO_2 uptake of, respectively, 195 and 170 mg g^{-1} (Yuan et al., 2020). These values are in the same order as reported in another study, also revalorizing PET bottles, and applying diverse activating agents such as KOH, H_3PO_4, $ZnCl_2$, and H_2SO_4 (Adibfar et al., 2014). The KOH-activated char led to the best performance, establishing a retention of 110 mg CO_2 g^{-1}, and a CO_2 uptake sequence by activating agents of KOH > H_3PO_4 > $ZnCl_2$ > H_2SO_4. Polyurethane has reported the highest CO_2 capacity, 293 mg g^{-1} (273 K), after activation with KOH, highly linked to the extremely microporous developed porosity (Ge et al., 2016). In this work, the maximum CO_2 uptake (130.2 mg g^{-1}) was defined by the activation with K_2CO_3, lower than the values reported in the literature for residue composed of one polymer type. It should be considered that the waste used in this work was a complex mixture of plastic waste with no further practical separation since it comes from the rejected fraction of municipal solid waste.

The thermodynamic behavior was assessed by monitoring the isotherms for either CO_2 or CH_4 at 273 and 298 K, allowing the obtention of the isosteric adsorption heat. Fig. 6 depicts the CO_2 isotherms at both temperatures, which defined a growing increase explainable by the Freundlich model (R^2> 0.99) with the lack of a well-defined plateau. The empirical Freundlich model describes non-ideal and reversible adsorption onto a monolayer or multilayer packing on a heterogeneous surface (Freundlich, 1907). The expected exothermicity of the process was corroborated by a decreasing CO_2 uptake with the increase in the operating temperature. The adsorption behavior pertaining to the chemical activating agent described the order of micropore volume: K_2CO_3 > KOH > Na_2CO_3 > NaOH > $ZnCl_2$ > $FeCl_3$; being the uptake of the non-activated char negligible. Table 2 summarizes the CO_2 uptake at near ambient pressure of the chars carbonized at 450 and 500 °C, further confirming the benefits of the higher carbonization temperature on the CO_2 uptake. The IAST selectivity of simulated exhausted fuel fumes with

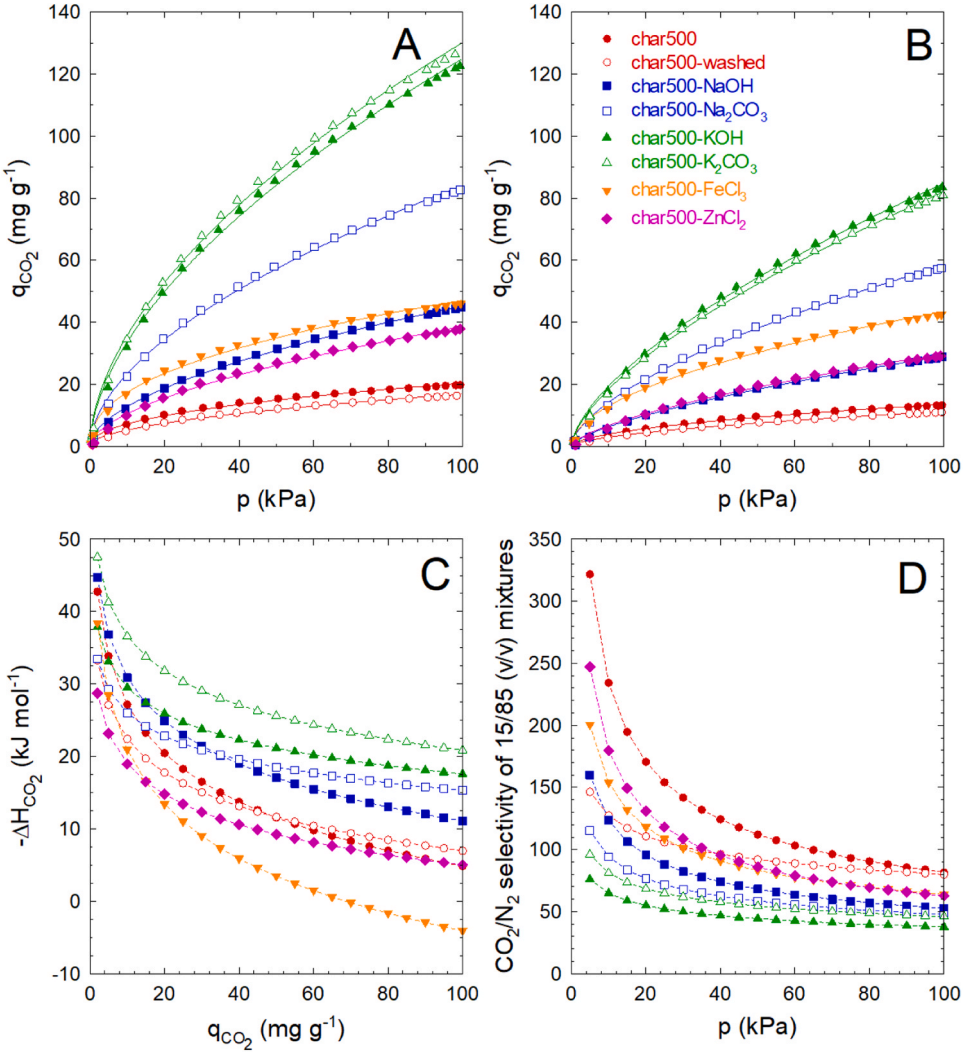

Fig. 6. Influence of the activating agent on the CO_2 uptake of chars carbonized at 500 °C at 0 °C (A) and 25 °C (B). Isosteric heat of CO_2 adsorption as a function of the pressure (C) and IAST CO_2/N_2 selectivity at 25 °C of 15/85 (v/v) mixtures (D) and. *The lines of subFigs. A and B depict the fitting to the Freundlich model.*

a 15/85 ratio of CO_2/N_2. The non-activated char displayed, although adsorbed very low CO_2, showed the highest selectivity, probably due to the negligible N_2 uptake at 298 K. depicted in Fig. 6 C, decreased as the strong active sites of the surface are covered as pressure raises, a consequence of the heterogeneity of the sample. The Freundlich model assumes a logarithmic decrease of the adsorption energy with the number of available adsorption sites. All the obtained values were below 40 kJ mol^{-1}, typically described as physisorption interaction (Saleh, 2022). Interestingly, the adsorption heat of CO_2, all exothermic except for the activation with $FeCl_3$, followed the same order registered for CO_2 performance: K_2CO_3 > KOH > Na_2CO_3 > NaOH > $ZnCl_2$ > $FeCl_3$; supported from a thermodynamic perspective the behavior among the samples. The activated sample depicted selectivity values (Fig. 6 D) in the same order of magnitude, being those activated with chlorides the most selective in this sense ($S_{CO2/N2}$ values at 100 kPa): $ZnCl_2$ (64) ~ $FeCl_3$ (63) > NaOH (53) > Na_2CO_3 (48) > K_2CO_3 (46) > KOH (38).

Similarly, the CH_4 uptake behavior was also assessed on the chars carbonized at 500 °C after different activating agents, see Fig. 7. Interestingly, some changes are depicted among the most active samples, i.e. the order for CH_4 adsorption followed was KOH > K_2CO_3 > Na_2CO_3 > $FeCl_3$ > NaOH > $ZnCl_2$, which implies a better selectivity of the sample activated with K_2CO_3 versus KOH in CO_2/CH_4 mixtures. The selectivity of simulated biogas with 40/60 (v/v) of CO_2/CH_4 was higher for the activation with K_2CO_3 and KOH as illustrated in Fig. 7 D, displaying the highest value with $ZnCl_2$. The thermodynamics also supported this tendency, the KOH displayed a slightly higher adsorption heat of CH_4 than the K_2CO_3 and the $ZnCl_2$ the lowest value, explaining a poorer interaction of CH_4 with the surface and the highest selectivity of CO_2/CH_4 mixtures.

The CO_2 adsorption mechanism onto porous carbonaceous materials has been described through van der Waals forces, whereas the presence of surface functional groups promotes the adsorption via electrostatic forces (Varghese et al., 2023). Thus, van der Waals interactions outline in narrow pores as the molecule can increase the potential interaction with multiple points from the adjacent walls of the pore (Sevilla et al., 2013). It has been described in the literature that CO_2 adsorption on

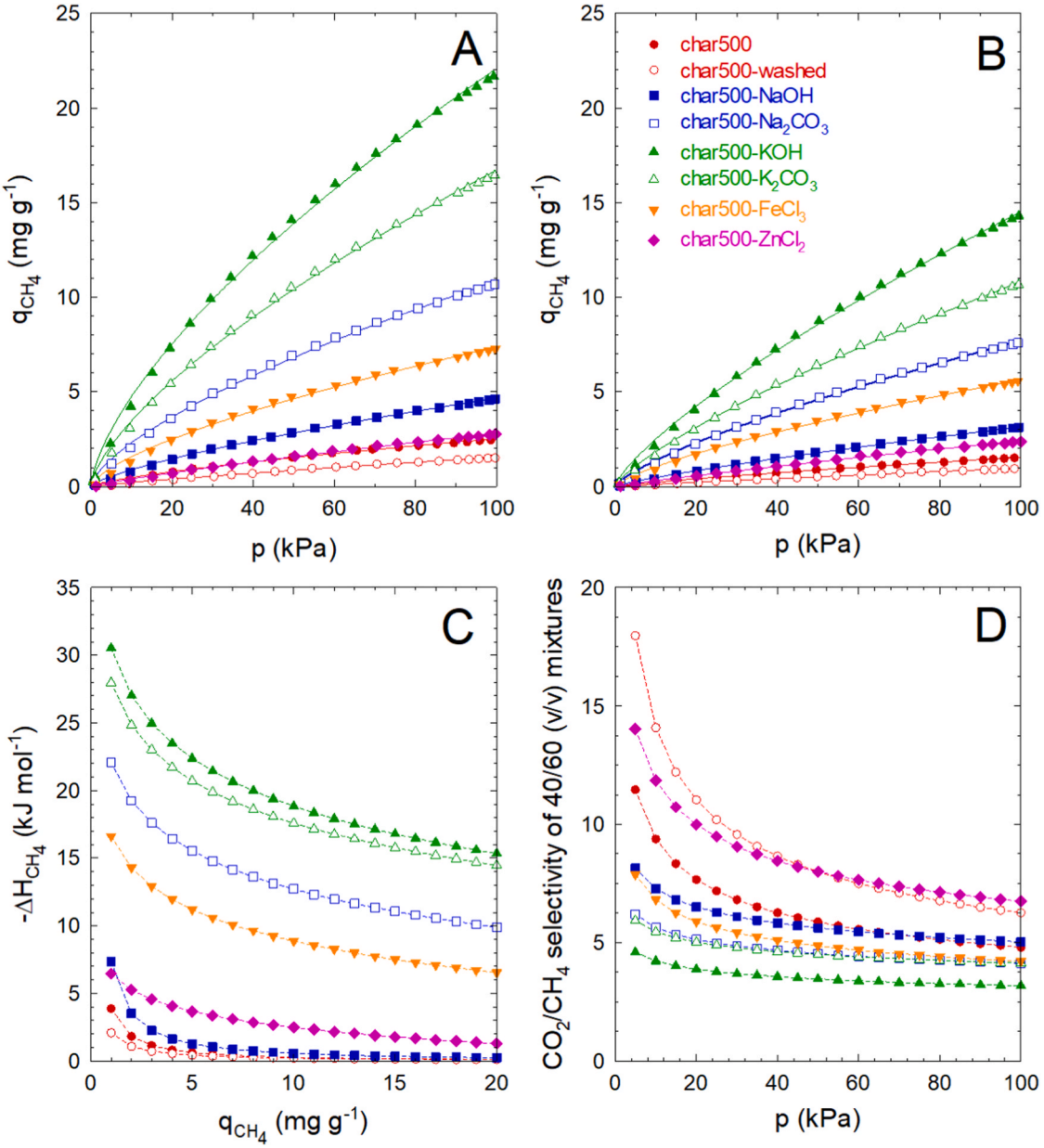

Fig. 7. Influence of the activating agent on the CH_4 uptake of chars carbonized at 500 °C at 0 °C (A) and 25 °C (B). Isosteric heat of CH_4 adsorption as a function of the pressure (C) and IAST CO_2/CH_4 selectivity at 25 °C of 40/60 (v/v) mixtures (D). *The lines of subFigs. A and B depict the fitting to the Freundlich model.*

activated carbons takes place typically in volume-filling rather than surface coverage, as happens with mesoporous materials. Consequently, the micropore size is quite important, being the optimum value described as twice the size of the adsorbate, i.e., as CO_2 size is around 0.33 nm the optimum micropore size should be roughly 0.7–0.8 nm (Varghese et al., 2023). Fig. 8 delineates the effect of CO_2 uptake (273 K and 100 kPa) versus the ultra-micropore volume, i.e. inferior to 1 nm, or the percentage of the oxygenated surface area of micropores estimating the surface oxygenated contribution by XPS analysis for all the plastic-chars activated at 500 ºC. Regarding the relationship of q_{CO2} and V_{MP} (<1 nm), it is observed a good linear correlation between the two variables, as reported in other precursors such as biomass in the literature (Varghese et al., 2023), except for the non-activated chars or the char-activated with $FeCl_3$, whose CO_2 uptake goes far from the predicted tendency. This abnormally high CO_2 uptake of these poorly micropore samples may be caused by other different reasons than the existence of micropores. As a matter of fact, it has been claimed that $FeCl_3$ displays a high ability to develop oxygenated surface groups. The Fe_2O_3 produced during the activation process reacts with carbon, leading to the formation of oxygenated groups and Fe_3O_4 (Bedia et al., 2020). Accordingly, the CO_2 uptake results are better explained based on the oxygenated surface of micropores. Therefore, the integrated interaction of van de Waals forces in micropores below 1 nm and the presence of oxygenated groups that contribute via electrostatic interaction better explains the results achieved with the different activating chemicals.

3.3. Dynamic adsorption tests of CO_2 and CH_4 and their mixtures

As a first screening test, the behavior of the different chemical activating agents on the dynamic tests was carried out in a fixed-bed column with the chars carbonized at 500 ºC, due to the better performance as previously stated. Fig. 9 depicts the breakthrough curves obtained feeding an inlet gas stream composed of a mixture of 40/60 (v/v) of CO_2/N_2. From the results attained in this figure, a similar behavior concerning the assays conducted under static mode is obtained, being the two most effective samples those activated with K_2CO_3 and KOH, in which K_2CO_3 performs the best CO_2 retention.

Regarding the results achieved, excellent performance was observed with the char activated with K_2CO_3 very convenient as this activating agent is considered a harmless and greener chemical. Compared to KOH, K_2CO_3 is a milder alkali compound, less toxic, and more corrosive (Sevilla et al., 2021). Also, to our knowledge, there is scarce information in the literature about the preparation of activated carbons based on plastic waste by chemical impregnation using K_2CO_3 as an activating agent, neither their application for CO_2 nor CH_4 adsorption. Accordingly, the plastic-based activated carbon prepared with K_2CO_3 was selected for a further and detailed study on dynamic adsorption tests, aimed at analyzing the influence of CO_2 or CH_4 composition in their corresponding CO_2/N_2 or CH_4/N_2 mixtures. Hence, the CO_2/N_2 or CH_4/N_2 ratios varied from 20/80–80/20 (v/v), leading to the breakthrough curves illustrated in Fig. 10 and the main characteristic parameters in Table 6.

As expected, the breakthrough times shown in Table 6 were higher in the case of CO_2 than CH_4 due to the higher selectivity, which was translated into higher adsorption capacity. As the adsorbate concentration, either CO_2 or CH_4, increased, the breakthrough time gradually decreased. For instance, in the case of CO_2, the breakthrough time decreased from 55 to 41 s, whereas for CH_4 was from 32 to 25 s. This indicates that by increasing the initial concentration of the adsorbate, the column saturates faster and the volume of treated gas, delimited by the breakpoint, is lower. Besides, the adsorption capacity was enlarged with increasing adsorbate concentration in the inlet effluent. For example, in the case of CO_2, the values moved from 55.3 mg g^{-1} (20/80 of CO_2/N_2) to 125.3 mg g^{-1} (80/20 of CO_2/N_2). Similarly, although with lower values, in the case of CH_4, the adsorption capacity also rose from 8.6 mg g^{-1} (20/80 of CH_4/N_2) to 26.2 mg g^{-1} (80/20 of CH_4/N_2).

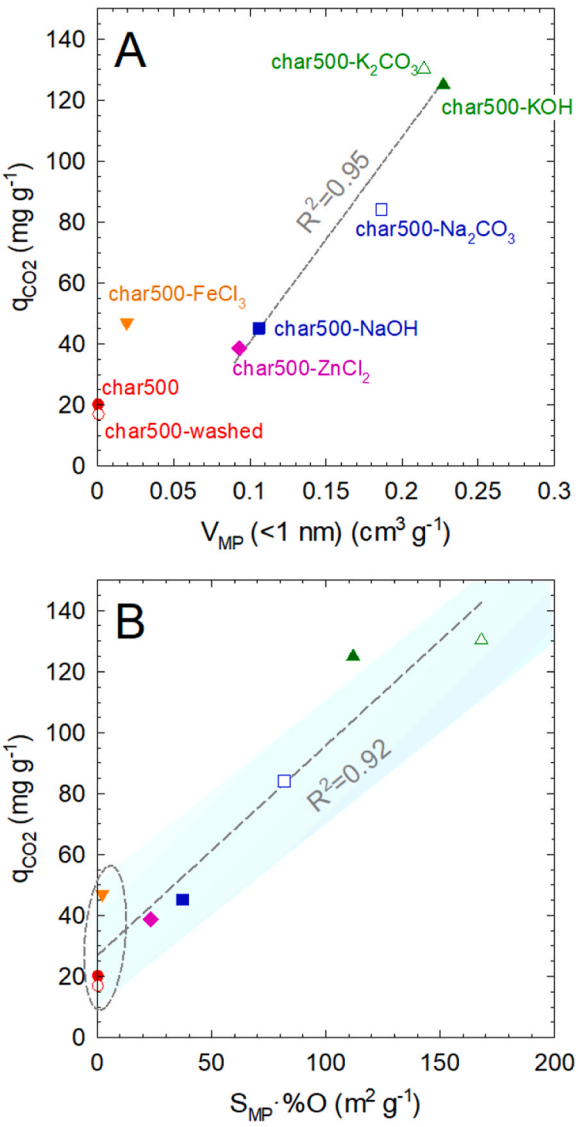

Fig. 8. Correlation of the CO_2 adsorption uptake (273 K and 100 kPa) vs ultra-micropore volume HK method (A), and correlation of the CO_2 adsorption uptake (273 K and 100 kPa) and the percentage of oxygenated micropores (B) for the plastic-based activated carbon prepared from the pyrolyzed char at 500 ºC.

This positive effect is commonly observed in dynamic tests on a fixed-bed column (Ligero et al., 2023a). The benefits exerted by inlet adsorbate concentration on the adsorbate uptake can be justified based on a greater probability of several adsorbate molecules interacting with the active points of the adsorbent (Hook, 1997; Tan et al., 2014). Subsequently, the higher the adsorbate concentration gradient, the lower the resistance to the mass transfer, launching the driving force for the adsorption process. Additionally, if the gas uptake obtained in the dynamic tests is compared to the static assays, some slight differences are observed, in the case of CO_2 the values were 82.1 mg g^{-1} (static) versus 125.3 mg g^{-1} (dynamic), and CH_4 displayed 10.7 mg g^{-1} (static) versus 27.2 mg g^{-1} (dynamic). The usually overestimated values depicted by dynamic tests if compared to static assays may be attributed to the different operating fluid dynamics in each case (Pu et al., 2021; Ramos et al., 2022). Where the sample was static and inside the cell in the static assays, in the fixed-bed setup the contact is more favorable since the gas is forced to cross the adsorbent, increasing the possibility of gas retention.

To assess the behavior of the optimum material, i.e. char500-K_2CO_3, some assays were conducted in CH_4/CO_2 mixtures to simulate the biogas

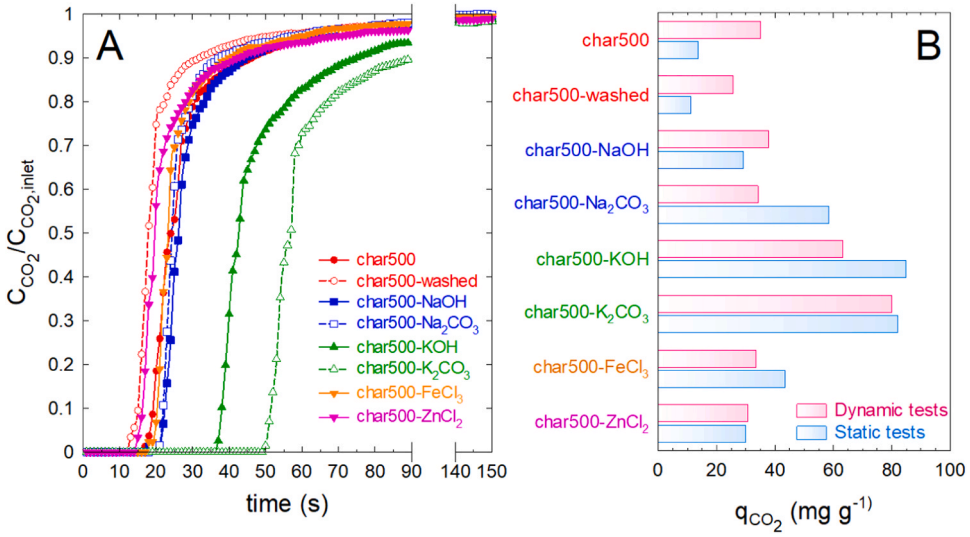

Fig. 9. Breakthrough curves of the plastic-based activated carbons prepared from the chars carbonized at 500 ºC under 40/60 (v/v) CO_2/N_2 mixtures at 298 K (A) and the comparison of the CO_2 uptake from dynamic and static tests (B) at atmospheric pressure.

composition for real practical application. Since the content of CH_4 in biogas usually exceeds 50 % (Benato and Macor, 2019; Calbry-Muzyka et al., 2022; Y. Li et al., 2019a; Rasi et al., 2007), 50/50, 60/40, 70/30, and 80/20 (v/v) CH_4/CO_2 mixtures were carried out. The breakthrough curves of CO_2 and CH_4 are depicted in Fig. 11 whereas the main characteristic parameter extracted from the curves are available in Table 7.

As expected by the higher CO_2 selectivity, the curves depicted in Fig. 11 define first the appearance of CH_4, followed by CO_2 after saturation. The quality of separation is provided by the difference period defined by the breaking times of both components, in which the material is already saturated in CH_4, but still absorbing CO_2, leading to a gas outlet enriched in CH_4. From a practical point of view, the time of a continuously operating process cycle is determined by the difference between the breaking times (t_{breat}) of both components. Moreover, it is observed that there is a sharp increase in the output of CH_4, reaching values higher than the input concentration of CH_4 which can reach values above up to 100 % in some cases to further decrease until reaching the saturation conditions (t_{sat}). As CO_2 is adsorbed, the outlet gas is enriched in CH_4, reaching theoretical values of 100 % CH_4 if all the CO_2 is retained.

The selective adsorption of solid porous adsorbents helps the separation of CH_4-CO_2 mixtures and mostly results from one or more of the following mechanisms: thermodynamic equilibrium effect, steric effect, and kinetic effect. Strongly adsorbed molecules are separated from weakly adsorbed molecules during adsorption according to the equilibrium effect, which might happen due to the different adsorbate molecules' attraction to the adsorbent surface. An adsorption-based separation can also be based on the size and the shape of the guest molecules, in which small molecules are adsorbed with a kinetic diameter smaller than the pores, leaving larger particles unadsorbed due to steric impediment. Finally, while the affinity is decisive in equilibrium

Table 6
Adsorption parameters evaluated from breakthrough curves of CO_2 and CH_4 with char500-K_2CO_3 under CO_2/N_2 and CH_4/N_2 mixtures.

Mixture	Composition (v/v)	t_{break} (s)	t_{sat} (s)	Removal (%)	q (mg g^{-1})
CO_2/N_2	20/80	55	207	40.8	55.3
	40/60	51	122	49.8	79.5
	60/40	42	80	61.3	96.3
	80/20	41	77	57.0	125.3
CH_4/N_2	20/80	32	60	66.8	8.6
	40/60	29	53	63.5	16.0
	60/40	27	41	74.3	21.7
	80/20	25	40	71.4	27.2

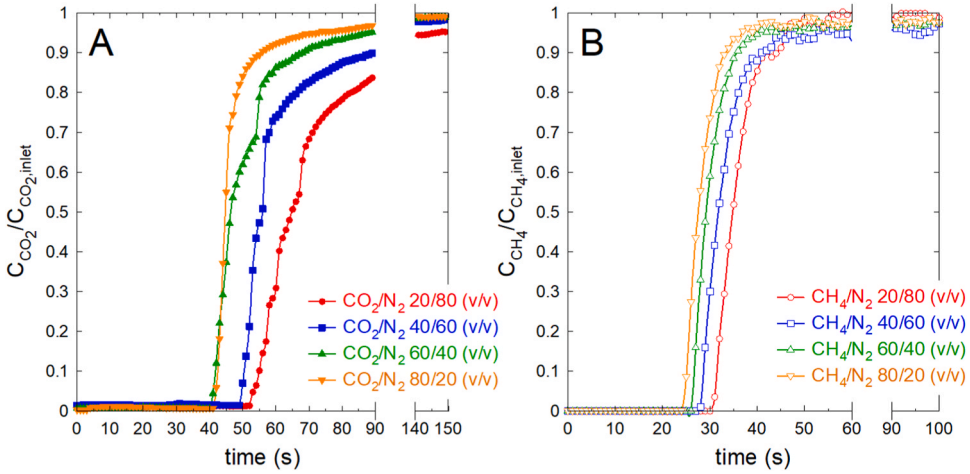

Fig. 10. Breakthrough curves of CO_2 and CH_4 with char500-K_2CO_3 under CO_2/N_2 (A) and CH_4/N_2 mixtures (B).

separation, kinetic separation is highly dependent on the rate at which the adsorbed molecules, with different sizes and shapes, can diffuse in the solid structure (Fakhraei Ghazvini et al., 2021). However, the precise mechanism should be studied in detail, and only then more specific predictions can be made for industry-scale process design (Lu et al., 2014). Some specific chemical groups of the plastic-based activated carbons, e.g. mainly oxygen functional groups, prefer to adsorb CO_2 over the CH_4 molecules, which increases the selectivity for CO_2 molecules. Also, the separation performance in activated carbons was greatly affected by the nature of the pores of the materials. The increasing microporous surface and binding sites let greater adsorption of CO_2 than CH_4 due to the stronger quadrupole moment and polarizability of CO_2, leaving a much more disadvantageous environment for CH_4 adsorption (Yu et al., 2019).

Fig. 12 depicts that the plastic-based activated char500-K_2CO_3 displays very close profiles to the commercial zeolite formula used in biogas upgrading when feeding 50/50 mixtures. In this case, the difference in breaking times between CH_4 and CO_2 is 9 s of the char500-K_2CO_3 versus the 15 s provided by the commercial zeolite. Bearing in mind that the plastic-based adsorbent was prepared from a valorized residue, the different adsorption mechanisms as a molecular sieve, and the higher cost of the zeolite, the prepared material seems very competitive for the upgrading application. At a higher proportion of CH_4 in the feeding gas, the zeolite was demonstrated to be more effective than the carbonaceous material, enlarging the breaking time between CH_4 and CO_2, and therefore the operating time. From the textural properties of the zeolitic molecular sieve and the comparison with the char500-K_2CO_3, see Fig. 12, it is appreciated that the zeolite exhibits lower total surface area than the plastic-based activated carbon, i.e. 446.3 versus 803.7 $m^2\ g^{-1}$, respectively. Additionally, the micropore volume of the carbon material is also higher, 0.221 (zeolite) versus the 0.307 $cm^3\ g^{-1}$ (char500-K_2CO_3). However, from the pore size distribution, the zeolite clearly states a narrower frequent ultramicropore size centered at 0.371 nm, an aspect of paramount importance that strongly impacts the CO_2 uptake, reaching values at 100 kPa of 218.9 mg g^{-1} (273 K) and 162.5 mg g^{-1} (298 K). The narrow pore size effectively acts as a molecular sieve and impedes the penetration of CH_4 molecules of bigger size than CO_2; subsequently, the CH_4 uptake is lower than the registered with the carbon-based material, sky-rocketing the selectivity towards CO_2, i.e. around 48 a 1000 kPa. However, the high cost of zeolites makes carbonaceous materials competitive although it implies a reduction of selectivity, the comparison of the char500-K_2CO_3 CO_2/CH_4 selectivity of 3.2 is quite close to the 4.7 reported for commercial formulas that display similar micropore size, i.e. 0.8 nm, prepared by activated by physical methods (Peredo-Mancilla et al., 2019).

The tendency observed in the enlarged breaking times at raising the CH_4 at the inlet stream evidences a rising value of the CH_4 yield, see Table 7. This fact evidences the lower CH_4 yield reached at rising the CH_4 concentration fed to the column. Comparing the yield performed by the zeolite to the plastic-based activated carbon, the values are over 3-folded. The performance of novel activated carbon is still lower than that of commercial zeolite. However, if compared to the values reported in the literature with other carbon materials, the char500-K_2CO_3 exhibits a very similar value to activated carbon prepared from biomass

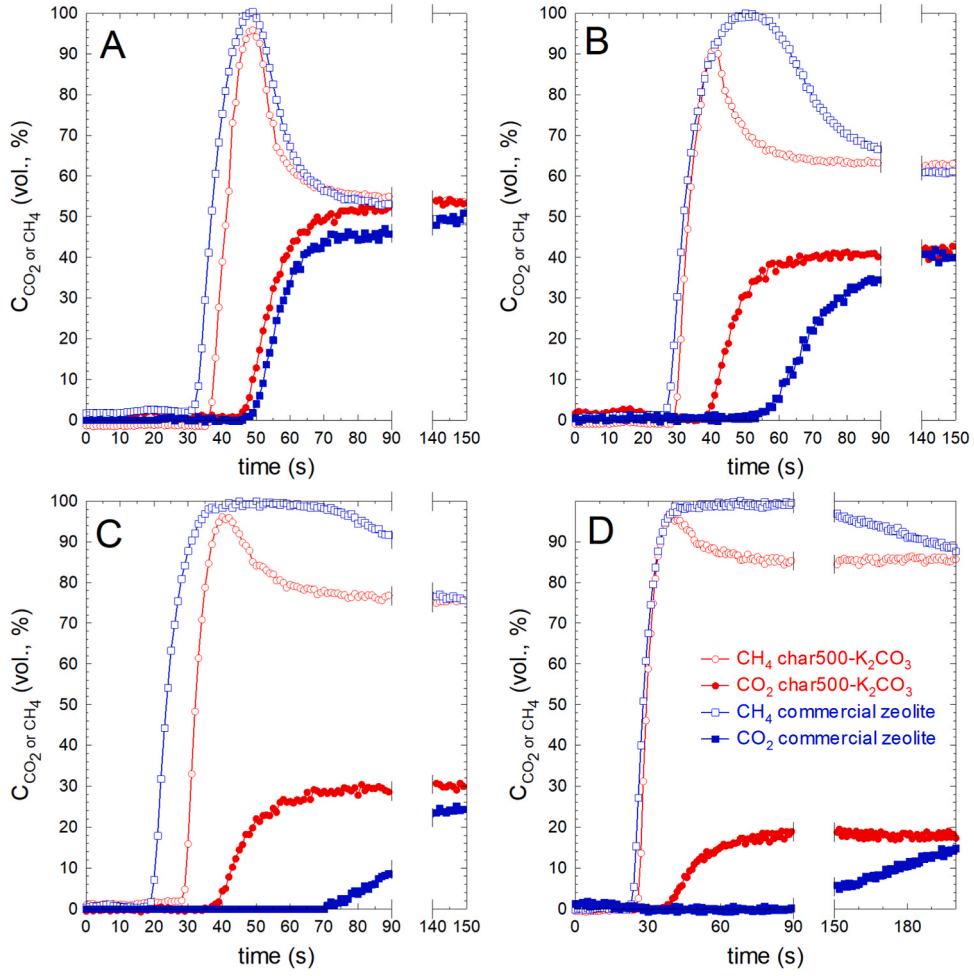

Fig. 11. Breakthrough curves CO_2 and CH_4 with char500-K_2CO_3 and commercial zeolite under different CO_2/CH_4 (v/v) mixtures, 50/50 (A), 40/60 (B), 30/70 (C) and 20/80 (D).

Table 7
Adsorption parameters evaluated from breakthrough curves of CO_2 and CH_4 with char500-K_2CO_3 under CO_2/CH_4 mixtures.

Material	CO_2/CH_4 (v/v)	CO_2				CH_4				Y_{CH4} (mmol g^{-1} min^{-1})	CH_4 Purity (%)	CH_4 Recovery (%)
		t_{break} (s)	t_{sat} (s)	R (%)	q (mg g^{-1})	t_b (s)	t_{ex} (s)	R (%)	q (mg g^{-1})			
Char500-K_2CO_3	50/50	46	74	73.3	86.4	37	42	94.4	23.6	0.146	94.3	6.5
	40/60	39	77	64.8	59.3	30	36	88.7	22.8	0.163	80.4	6.1
	30/70	39	83	74.7	46.9	27	34	87.2	25.4	0.360	93.4	11.5
	20/80	38	84	62.0	34.5	26	33	87.5	27.5	0.653	93.8	18.3
Zeolite 13X	50/50	47	99	60.9	98.8	32	36	89.1	19.6	0.243	99.7	10.9
	40/60	54	104	61.7	94.5	27	33	89.0	21.0	0.550	99.8	20.5
	30/70	72	169	57.6	112.5	19	26	84.5	18.3	1.166	99.9	37.3
	20/80	126	250	70.2	114.9	24	32	82.8	27.7	2.367	99.8	66.3

precursors, such as cherry stone (Álvarez-Gutiérrez et al., 2016) and coconut shell (Bałys et al., 2021), or commercial activated carbon formulas (Bałys et al., 2021).

This CH_4 enrichment capability of our plastic-based activated carbons has potential implications and applications in the energy transition through renewable fuel production since it can lead to the production of biomethane. The qualities and applications of biomethane gas are like those of natural gas, making it a versatile and easy-to-store fuel that doesn't require natural gas equipment and device settings to be changed. It can be utilized for both residential and industrial purposes, including direct power generation in hydrogen or biomethane fuel cells, feedstock for Fischer-Tropsch fuel manufacturing processes, and thermal and power generation (Koonaphapdeelert et al., 2020).

Recycling and regeneration of char500-K_2CO_3 was also evaluated since it is important for successfully commercializing new adsorbent materials. Fig. 13 depicts the CO_2 and CH_4 capacity and the CO_2 recovery of char500-K_2CO_3 after five adsorption-desorption cycles. The adsorption capacities were constant on the first five regeneration cycles. The constant adsorption capacities after regeneration can be ascribed to the successful adsorbent regeneration. It has been reported that some other common adsorbent materials such as activated carbons and zeolites maintain good adsorption performance up to or more than five regeneration cycles (Fayaz et al., 2015; Giraudet et al., 2014; Kim and Ahn, 2012; Wang et al., 2012; Zaitan et al., 2016).

4. CONCLUSIONS

This work proves the feasibility of valorisation of plastic waste of mixed polymers unsuitable for mechanical recycling. The carbonization temperature at which the plastic char was obtained exerted a positive effect on the second stage of activation, being the results attained at 500 °C better than at 450 °C. From the different chemical activating agents studied, the use of less toxic K_2CO_3 displayed better results than KOH either on the textural properties and CO_2 adsorption capacity. The sodium salts lead to poorer results if compared to their potassium counterparts. $ZnCl_2$ and $FeCl_3$ failed in the development of textural properties and CO_2 uptake. All the activating agents lead to micropores of an average size centered at roughly 0.75 nm. The percentage of ultramicropores and oxygenated surface groups were well-correlated with the CO_2 uptake, being the highest value obtained with K_2CO_3 either in static and dynamic adsorption experiments, with respective values at 25 °C of 82.1 and 79.5 mg g^{-1}.

The breakthrough curves over CO_2/CH_4 mixtures of 50/50 (v/v) depicted close behavior to commercial materials such as zeolites, although at higher CH_4 proportion the higher selectivity of the zeolite due to the molecular sieve mechanism with micropores of lower than 0.5 nm that allows the insertion of CO_2 nor CH_4 launched the benefits if compared to the plastic-based activated carbon. However, if the results are compared to other carbon formulas, either commercial or prepared from other precursors such as biomass, the results of the valorized plastic waste are very competitive, reaching comparable CH_4 production yield in the obtention of a CH_4 stream enriched at 95 %.

Recycling and regeneration of char500-K_2CO_3 were also evaluated after five adsorption-desorption cycles. The constant adsorption capacities after regeneration can be ascribed to the successful adsorbent regeneration.

Some future strategies to improve the performance of plastic-based activated carbons include: i) develop a comprehensive roadmap for

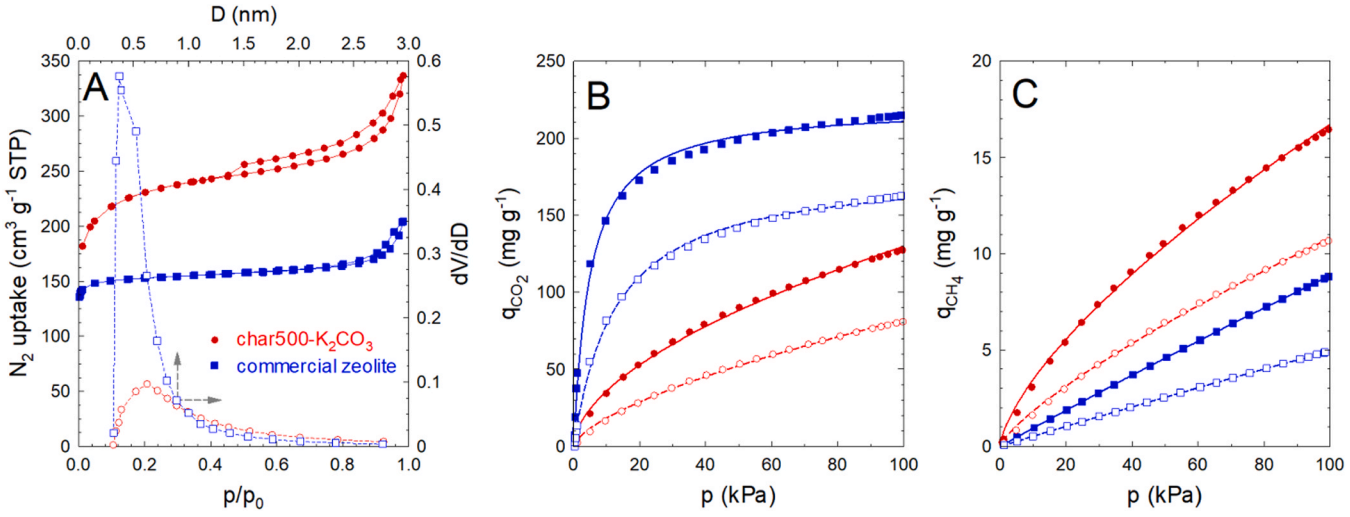

Fig. 12. Comparison of commercial formulas and char500-K_2CO_3 for biogas upgrading. N_2 adsorption-desorption isotherms and micropore size distribution (A), CO_2 isotherms, and CH_4 isotherms (B) at 273 K (filled symbols) and 298 K (empty symbols). *Connecting lines of subFigs. B and C represent the fitting to Freundlich (char500-K_2CO_3) and Langmuir (zeolite) models.*

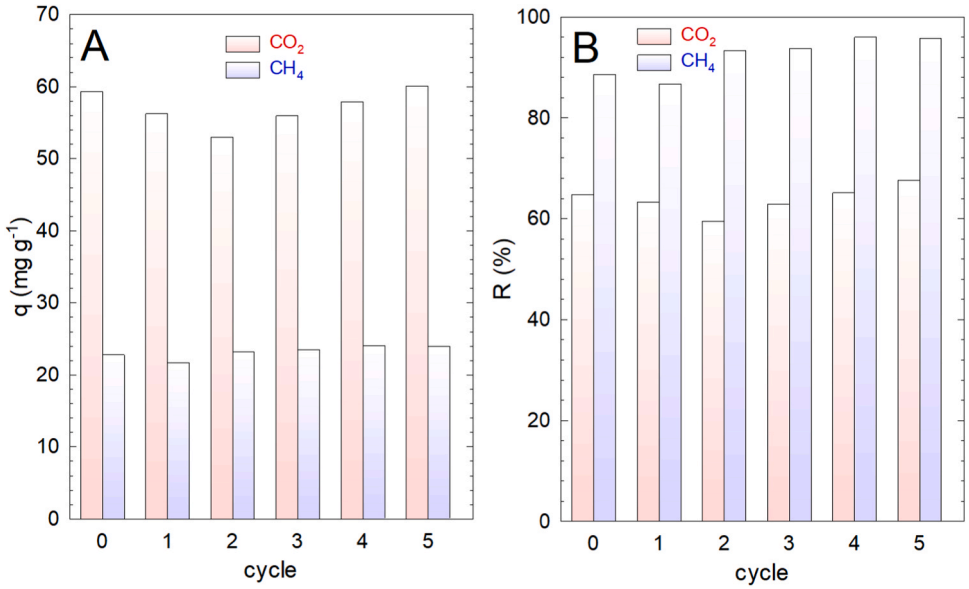

Fig. 13. Adsorption parameters during sequential cycles with char500-K_2CO_3 under a CO_2/CH_4 mixture 40/60.

implementing new precursors and technologies in activated carbon production; ii) incorporate new techniques and technologies to improve the production process and increase efficiency; iii) investigate the performance of plastic-based activated carbon in other applications.

CRediT authorship contribution statement

Rafael R. Solís: Writing – review & editing, Writing – original draft, Formal analysis, Data curation, Conceptualization, Investigation. **Gabriel Blázquez:** Validation, Supervision, Resources, Methodology, Investigation. **Sandra Ramirez:** Methodology, Investigation. **Ledicia Pereira:** Methodology, Investigation. **Mónica Calero:** Writing – review & editing, Supervision, Project administration, Funding acquisition, Formal analysis. **M.A. Martín-Lara:** Writing – review & editing, Writing – original draft, Supervision, Project administration, Funding acquisition, Formal analysis.

Declaration of Competing Interest

The authors declare that they have no known competing financial interests or personal relationships that could have appeared to influence the work reported in this paper.

Acknowledgments

The authors acknowledge the Ministry of Science and Innovation and the Research State Agency (10.13039/501100011033), and the European Union Next Generation EU/PRTR, Projects Oriented to Ecological and Digital Transition 2021 for the project TED2021–130157B-I00, CARBOPLASTIC. They also thank the support provided for the external services of investigation of the University of Granada (Centro de Instrumentación Científica. CIC). The authors also acknowledge the Sysadvance company for the technical support provided to carry out this work. Funding for open access charge: Universidad de Granada / CBUA.

References

Abbas, A.F., Ahmed, M.J., 2016. Mesoporous activated carbon from date stones (Phoenix dactylifera L.) by one-step microwave assisted K_2CO_3 pyrolysis. J. Water Process Eng. C. 201–207. https://doi.org/10.1016/J.JWPE.2016.01.004.

Adibfar, M., Kaghazchi, T., Asasian, N., Soleimani, M., 2014. Conversion of poly (ethylene terephthalate) waste into activated carbon: chemical activation and characterization. Chem. Eng. Technol. 37, 979–986. https://doi.org/10.1002/CEAT.201200719.

Adrados, A., de Marco, I., Caballero, B.M., López, A., Laresgoiti, M.F., Torres, A., 2012. Pyrolysis of plastic packaging waste: A comparison of plastic residuals from material recovery facilities with simulated plastic waste. Waste Manag. 32, 826–832. https://doi.org/10.1016/J.WASMAN.2011.06.016.

Ahmed, S., Parvaz, M., Johari, R., Rafat, M., 2018. Studies on activated carbon derived from neem (Azadirachta indica) bio-waste, and its application as supercapacitor electrode. Mater. Res Express 5, 045601. https://doi.org/10.1088/2053-1591/AAB924.

Ahmed, M.J., Theydan, S.K., 2012. Adsorption of cephalexin onto activated carbons from Albizia lebbeck seed pods by microwave-induced KOH and K_2CO_3 activations. Chem. Eng. J. 211–212 200–207. https://doi.org/10.1016/J.CEJ.2012.09.089.

Alhamed, Y.A., 2009. Adsorption kinetics and performance of packed bed adsorber for phenol removal using activated carbon from dates' stones. J. Hazard Mater. 170, 763–770. https://doi.org/10.1016/J.JHAZMAT.2009.05.002.

Alvarez, J., Lopez, G., Amutio, M., Bilbao, J., Olazar, M., 2015. Physical Activation of Rice Husk Pyrolysis Char for the Production of High Surface Area Activated Carbons. Ind. Eng. Chem. Res 54, 7241–7250. https://doi.org/10.1021/ACS.IECR.5B01589.

Álvarez-Gutiérrez, N., García, S., Gil, M.V., Rubiera, F., Pevida, C., 2016. Dynamic Performance of Biomass-Based Carbons for CO_2/CH_4 Separation. Approximation to a Pressure Swing Adsorption Process for Biogas Upgrading. Energy Fuels 30, 5005–5015. https://doi.org/10.1021/ACS.ENERGYFUELS.6B00664.

Ariyadejwanich, P., Tanthapanichakoon, W., Nakagawa, K., Mukai, S.R., Tamon, H., 2003. Preparation and characterization of mesoporous activated carbon from waste tires. Carbon N. Y 41, 157–164. https://doi.org/10.1016/S0008-6223(02)00267-1.

Bałys, M., Brodawka, E., Jodłowski, G.S., Szczurowski, J., Wójcik, M., 2021. Alternative Materials for the Enrichment of Biogas with Methane. Materials 14, 7759. https://doi.org/10.3390/MA14247759.

Bang, J.H., Lee, H.M., An, K.H., Kim, B.J., 2017. A study on optimal pore development of modified commercial activated carbons for electrode materials of supercapacitors. Appl. Surf. Sci. 415, 61–66. https://doi.org/10.1016/J.APSUSC.2017.01.007.

Bedia, J., Peñas-Garzón, M., Gómez-Avilés, A., Rodriguez, J.J., Belver, C., 2020. Review on Activated Carbons by Chemical Activation with $FeCl_3$. C. J. Carbon Res. 6, 21. https://doi.org/10.3390/C6020021.

Beltrame, K.K., Cazetta, A.L., de Souza, P.S.C., Spessato, L., Silva, T.L., Almeida, V.C., 2018. Adsorption of caffeine on mesoporous activated carbon fibers prepared from pineapple plant leaves. Ecotoxicol. Environ. Saf. 147, 64–71. https://doi.org/10.1016/J.ECOENV.2017.08.034.

Benato, A., Macor, A., 2019. Italian Biogas Plants: Trend, Subsidies, Cost, Biogas Composition and Engine Emissions. Energ. (Basel) 12, 979. https://doi.org/10.3390/EN12060979.

Bian, Y., Yuan, Q., Zhu, G., Ren, B., Hursthouse, A., Zhang, P., 2018. Recycling of Waste Sludge: Preparation and Application of Sludge-Based Activated Carbon. Int J. Polym. Sci. 2018, 8320609 https://doi.org/10.1155/2018/8320609.

Biesinger, M.C., Lau, L.W.M., Gerson, A.R., Smart, R.S.C., 2010. Resolving surface chemical states in XPS analysis of first row transition metals, oxides and hydroxides: Sc, Ti, V, Cu and Zn. Appl. Surf. Sci. 257, 887–898. https://doi.org/10.1016/J.APSUSC.2010.07.086.

Burg, P., Fydrych, P., Cagniant, D., Nanse, G., Bimer, J., Jankowska, A., 2002. The characterization of nitrogen-enriched activated carbons by IR, XPS and LSER methods. Carbon N. Y 40, 1521–1531. https://doi.org/10.1016/S0008-6223(02)00004-0.

Calbry-Muzyka, A., Madi, H., Rüsch-Pfund, F., Gandiglio, M., Biollaz, S., 2022. Biogas composition from agricultural sources and organic fraction of municipal solid waste. Renew. Energy 181, 1000–1007. https://doi.org/10.1016/J.RENENE.2021.09.100.

de Paula, F.G.F., de Castro, M.C.M., Ortega, P.F.R., Blanco, C., Lavall, R.L., Santamaría, R., 2018. High value activated carbons from waste polystyrene foams. Microporous Mesoporous Mater. 267, 181–184. https://doi.org/10.1016/J.MICROMESO.2018.03.027.

Dombrowski, R.J., Lastoskie, C.M., Hyduke, D.R., 2001. The Horvath–Kawazoe method revisited. Colloids Surf. A Physicochem Eng. Asp. 187–188 23–39. https://doi.org/10.1016/S0927-7757(01)00618-5.

Durán, I., Rubiera, F., Pevida, C., 2022. Modeling a biogas upgrading PSA unit with a sustainable activated carbon derived from pine sawdust. Sensitivity analysis on the adsorption of CO_2 and CH_4 mixtures. Chem. Eng. J. 428, 132564 https://doi.org/10.1016/J.CEJ.2021.132564.

Esfandiari, A., Kaghazchi, T., Soleimani, M., 2012. Preparation and evaluation of activated carbons obtained by physical activation of polyethyleneterephthalate (PET) wastes. J. Taiwan Inst. Chem. Eng. 43, 631–637. https://doi.org/10.1016/J.JTICE.2012.02.002.

Eslami, A., Borghei, S.M., Rashidi, A., Takdastan, A., 2018. Preparation of activated carbon dots from sugarcane bagasse for naphthalene removal from aqueous solutions. Sep Sci. Technol. 53, 2536–2549. https://doi.org/10.1080/01496395.2018.1462832.

Espanani, R., Miller, A., Busick, A., Hendry, D., Jacoby, W., 2016. Separation of N_2/CO_2 mixture using a continuous high-pressure density-driven separator. J. CO_2 Util. 14, 67–75. https://doi.org/10.1016/J.JCOU.2016.02.012.

Fakhraei Ghazvini, M., Vahedi, M., Najafi Nobar, S., Sabouri, F., 2021. Investigation of the MOF adsorbents and the gas adsorptive separation mechanisms. J. Environ. Chem. Eng. 9, 104790 https://doi.org/10.1016/J.JECE.2020.104790.

Fayaz, M., Shariaty, P., Atkinson, J.D., Hashisho, Z., Phillips, J.H., Anderson, J.E., Nichols, M., 2015. Using microwave heating to improve the desorption efficiency of high molecular weight VOC from beaded activated carbon. Environ. Sci. Technol. 49, 4536–4542. https://doi.org/10.1021/ES505953C.

Feng, B., Shen, W., Shi, L., Qu, S., 2018. Adsorption of hexavalent chromium by polyacrylonitrile-based porous carbon from aqueous solution. R. Soc. Open Sci. 5 https://doi.org/10.1098/RSOS.171662.

Freundlich, H., 1907. Über die Adsorption in Lösungen. Z. F. üR. Phys. Chem. 57U, 385–470. https://doi.org/10.1515/ZPCH-1907-5723.

Gao, Y., Yue, Q., Gao, B., Li, A., 2020. Insight into activated carbon from different kinds of chemical activating agents: A review. Sci. Total Environ. 746, 141094 https://doi.org/10.1016/J.SCITOTENV.2020.141094.

Gauden, P.A., Terzyk, A.P., Rychlicki, G., Kowalczyk, P., Ćwiertnia, M.S., Garbacz, J.K., 2004. Estimating the pore size distribution of activated carbons from adsorption data of different adsorbates by various methods. J. Colloid Interface Sci. 273, 39–63. https://doi.org/10.1016/J.JCIS.2003.08.033.

Gayathiri, M., Pulingam, T., Lee, K.T., Sudesh, K., 2022. Activated carbon from biomass waste precursors: Factors affecting production and adsorption mechanism. Chemosphere 294, 133764. https://doi.org/10.1016/J.CHEMOSPHERE.2022.133764.

Ge, C., Song, J., Qin, Z., Wang, J., Fan, W., 2016. Polyurethane foam-based ultramicroporous carbons for CO_2 capture. ACS Appl. Mater. Interfaces 8, 18849–18859. https://doi.org/10.1021/ACSAMI.6B04771.

Giraudet, S., Boulinguiez, B., Le Cloirec, P., 2014. Adsorption and Electrothermal Desorption of Volatile Organic Compounds and Siloxanes onto an Activated Carbon Fiber Cloth for Biogas Purification. Energy Fuels 28, 3924–3932. https://doi.org/10.1021/EF500600B.

Gómez-Serrano, V., Adame-Pereira, M., Alexandre-Franco, M., Fernández-González, C., 2021. Adsorption of bisphenol A by activated carbon developed from PET waste by KOH activation. Environ. Sci. Pollut. Res. 28, 24342–24354. https://doi.org/10.1007/S11356-020-08428-6.

González-González, R.B., González, L.T., Iglesias-González, S., González-González, E., Martinez-Chapa, S.O., Madou, M., Alvarez, M.M., Mendoza, A., 2020. Characterization of Chemically Activated Pyrolytic Carbon Black Derived from Waste Tires as a Candidate for Nanomaterial Precursor. Nanomaterials 10, 2213. https://doi.org/10.3390/NANO10112213.

Gopinath, K.P., Vo, D.V.N., Gnana Prakash, D., Adithya Joseph, A., Viswanathan, S., Arun, J., 2021. Environmental applications of carbon-based materials: a review. Environ. Chem. Lett. 19, 557–582. https://doi.org/10.1007/S10311-020-01084-9.

He, S., Chen, G., Xiao, H., Shi, G., Ruan, C., Ma, Y., Dai, H., Yuan, B., Chen, X., Yang, X., 2021. Facile preparation of N-doped activated carbon produced from rice husk for CO_2 capture. J. Colloid Interface Sci. 582, 90–101. https://doi.org/10.1016/J.JCIS.2020.08.021.

Heidarinejad, Z., Dehghani, M.H., Heidari, M., Javedan, G., Ali, I., Sillanpää, M., 2020. Methods for preparation and activation of activated carbon: a review. Environ. Chem. Lett. 18, 393–415. https://doi.org/10.1007/S10311-019-00955-0.

Hook, R.J., 1997. An Investigation of Some Sterically Hindered Amines as Potential Carbon Dioxide Scrubbing Compounds. Ind. Eng. Chem. Res 36, 1779–1790. https://doi.org/10.1021/IE9605589.

Ilyas, M., Ahmad, W., Khan, H., 2021. Utilization of activated carbon derived from waste plastic for decontamination of polycyclic aromatic hydrocarbons laden wastewater. Water Sci. Technol. 84, 609–631. https://doi.org/10.2166/WST.2021.252.

Jamradloedluk, J., Lertsatitthanakorn, C., 2014. Characterization and Utilization of Char Derived from Fast Pyrolysis of Plastic Wastes. Procedia Eng. 69, 1437–1442. https://doi.org/10.1016/J.PROENG.2014.03.139.

Kaur, B., Gupta, R.K., Bhunia, H., 2019a. CO_2 capture on activated carbon from PET (polyethylene terephthalate) waste: Kinetics and modeling studies. Chem. Eng. Commun. 207, 1031–1047. https://doi.org/10.1080/00986445.2019.1635466.

Kaur, B., Singh, J., Gupta, R.K., Bhunia, H., 2019b. Porous carbons derived from polyethylene terephthalate (PET) waste for CO_2 capture studies. J. Environ. Manag. 242, 68–80. https://doi.org/10.1016/J.JENVMAN.2019.04.077.

Kim, K.J., Ahn, H.G., 2012. The effect of pore structure of zeolite on the adsorption of VOCs and their desorption properties by microwave heating. Microporous Mesoporous Mater. 152, 78–83. https://doi.org/10.1016/J.MICROMESO.2011.11.051.

Kim, J.W., Lee, H.G., 2001. Thermal and carbothermic decomposition of Na_2CO_3 and Li_2CO_3. Metall. Mater. Trans. B: Process. Metall. Mater. Process. Sci. 32, 17–24. https://doi.org/10.1007/S11663-001-0003-0.

Koonaphapdeelert, S., Aggarangsi, P., Moran, J., 2020. Production and Applications. Green Energy and Technology. In: Biomethane. Springer Singapore, Singapore. https://doi.org/10.1007/978-981-13-8307-6.

Koshizaki, N., Umehara, H., Oyama, T., 1998. XPS characterization and optical properties of Si/SiO_2, Si/Al_2O_3 and Si/MgO co-sputtered films. Thin Solid Films 325, 130–136. https://doi.org/10.1016/S0040-6090(98)00512-4.

Li, Y., Alaimo, C.P., Kim, M., Kado, N.Y., Peppers, J., Xue, J., Wan, C., Green, P.G., Zhang, R., Jenkins, B.M., Vogel, C.F.A., Wuertz, S., Young, T.M., Kleeman, M.J., 2019a. Composition and Toxicity of Biogas Produced from Different Feedstocks in California. Environ. Sci. Technol. https://doi.org/10.1021/ACS.EST.9B03003.

Li, S., Cho, M.K., Yuan, X., Deng, S., Li, H., Zhao, L., Zhao, R., Wang, Y., Wang, J., Lee, K. B., 2023. Cyclic performance evaluation of CO_2 adsorption using polyethylene terephthalate plastic-waste-derived activated carbon. Fuel 331, 125599. https://doi.org/10.1016/J.FUEL.2022.125599.

Li, H., Li, J., Thomas, A., Liao, Y., 2019b. Ultra-High Surface Area Nitrogen-Doped Carbon Aerogels Derived From a Schiff-Base Porous Organic Polymer Aerogel for CO_2 Storage and Supercapacitors. Adv. Funct. Mater. 29, 1904785 https://doi.org/10.1002/ADFM.201904785.

Li, Z.Q., Lu, C.J., Xia, Z.P., Zhou, Y., Luo, Z., 2007. X-ray diffraction patterns of graphite and turbostratic carbon. Carbon N. Y 45, 1686–1695. https://doi.org/10.1016/J.CARBON.2007.03.038.

Li, K., Ruan, H., Ning, P., Wang, C., Sun, X., Song, X., Han, S., 2018. Preparation of walnut shell-based activated carbon and its properties for simultaneous removal of H_2S, COS and CS_2 from yellow phosphorus tail gas at low temperature. Res. Chem. Intermed. 44, 1209–1233. https://doi.org/10.1007/S11164-017-3162-6.

Lian, F., Xing, B., Zhu, L., 2011. Comparative study on composition, structure, and adsorption behavior of activated carbons derived from different synthetic waste polymers. J. Colloid Interface Sci. 360, 725–730. https://doi.org/10.1016/J.JCIS.2011.04.103.

Liao, Y., Weber, J., Faul, C.F.J., 2015. Fluorescent microporous polyimides based on perylene and triazine for highly CO_2-selective carbon materials. Macromolecules 48, 2064–2073. https://doi.org/10.1021/MA501662R.

Ligero, A., Calero, M., Martín-Lara, M.Á., Blázquez, G., Solís, R.R., Pérez, A., 2023a. Fixed-bed CO_2 adsorption onto activated char from the pyrolysis of a non-recyclable plastic mixture from real urban residues. J. CO_2 Util. 73, 102517 https://doi.org/10.1016/J.JCOU.2023.102517.

Ligero, A., Calero, M., Pérez, A., Solís, R.R., Muñoz-Batista, M.J., Martín-Lara, M.Á., 2023b. Low-cost activated carbon from the pyrolysis of post-consumer plastic waste and the application in CO_2 capture. Process Saf. Environ. Prot. 173, 558–566. https://doi.org/10.1016/J.PSEP.2023.03.041.

Lillo-Ródenas, M.A., Cazorla-Amorós, D., Linares-Solano, A., 2003. Understanding chemical reactions between carbons and NaOH and KOH: An insight into the chemical activation mechanism. Carbon N. Y 41, 267–275. https://doi.org/10.1016/S0008-6223(02)00279-8.

Liu, Q., Jiang, S., Su, X., Zhang, X., Cao, W., Xu, Y., 2021. Role of the biochar modified with $ZnCl_2$ and $FeCl_3$ on the electrochemical degradation of nitrobenzene. Chemosphere 275, 129966. https://doi.org/10.1016/J.CHEMOSPHERE.2021.129966.

Lota, G., Centeno, T.A., Frackowiak, E., Stoeckli, F., 2008. Improvement of the structural and chemical properties of a commercial activated carbon for its application in electrochemical capacitors. Electro Acta 53, 2210–2216. https://doi.org/10.1016/J.ELECTACTA.2007.09.028.

Lozano-Castelló, D., Calo, J.M., Cazorla-Amorós, D., Linares-Solano, A., 2007. Carbon activation with KOH as explored by temperature programmed techniques, and the effects of hydrogen. Carbon N. Y 45, 2529–2536. https://doi.org/10.1016/J.CARBON.2007.08.021.

Lu, L., Wang, S., Müller, E.A., Cao, W., Zhu, Y., Lu, X., Jackson, G., 2014. Adsorption and separation of CO_2/CH_4 mixtures using nanoporous adsorbents by molecular simulation. Fluid Phase Equilib. 362, 227–234. https://doi.org/10.1016/J.FLUID.2013.10.013.

Ma, Y., 2017. Comparison of Activated Carbons Prepared from Wheat Straw via $ZnCl_2$ and KOH Activation. Waste Biomass-.-. Valoriz. 8, 549–559. https://doi.org/10.1007/S12649-016-9640-Z.

Martín-Lara, M.A., Piñar, A., Ligero, A., Blázquez, G., Calero, M., 2021. Characterization and Use of Char Produced from Pyrolysis of Post-Consumer Mixed Plastic Waste. Water (Basel) 13, 1188. https://doi.org/10.3390/W13091188.

Mendoza-Carrasco, R., Cuerda-Correa, E.M., Alexandre-Franco, M.F., Fernández-González, C., Gómez-Serrano, V., 2016. Preparation of high-quality activated carbon from polyethyleneterephthalate (PET) bottle waste. Its use in the removal of pollutants in aqueous solution. J. Environ. Manag. 181, 522–535. https://doi.org/10.1016/J.JENVMAN.2016.06.070.

Niksiar, A., Nasernejad, B., 2017. Activated carbon preparation from pistachio shell pyrolysis and gasification in a spouted bed reactor. Biomass-.-. Bioenergy 106, 43–50. https://doi.org/10.1016/J.BIOMBIOE.2017.08.017.

Ning, S.K., Hung, M.C., Chang, Y.H., Wan, H.P., Lee, H.T., Shih, R.F., 2013. Benefit assessment of cost, energy, and environment for biomass pyrolysis oil. J. Clean. Prod. 59, 141–149. https://doi.org/10.1016/J.JCLEPRO.2013.06.042.

Nuhnen, A., Janiak, C., 2020. A practical guide to calculate the isosteric heat/enthalpy of adsorption via adsorption isotherms in metal–organic frameworks, MOFs. Dalton Trans. 49, 10295–10307. https://doi.org/10.1039/D0DT01784A.

Otsuki, A., Shibayama, A., Sadaki, J., Fujita, T., Watanabe, M., 2007. Adsorption Properties of Activated Carbon Prepared from Waste Beer Lees by KOH Activation and CO_2 Activation. Resour. Process. 54, 19–24. https://doi.org/10.4144/RPSJ.54.19.

Parra, J.B., Ania, C.O., Arenillas, A., Rubiera, F., Pis, J.J., 2004. High value carbon materials from PET recycling. Appl. Surf. Sci. 238, 304–308. https://doi.org/10.1016/J.APSUSC.2004.05.229.

Peredo-Mancilla, D., Matei Ghimbeu, C., Ho, B.N., Jeguirim, M., Hort, C., Bessieres, D., 2019. Comparative study of the CH_4/CO_2 adsorption selectivity of activated carbons for biogas upgrading. J. Environ. Chem. Eng. 7, 103368 https://doi.org/10.1016/J.JECE.2019.103368.

Pereira, L., Castillo, V., Calero, M., Blázquez, G., Solís, R.R., Ángeles Martín-Lara, M., 2024. Conversion of char from pyrolysis of plastic wastes into alternative activated carbons for heavy metal removal. Environ. Res 250, 118558. https://doi.org/10.1016/J.ENVRES.2024.118558.

Pérez-Huertas, S., Calero, M., Ligero, A., Pérez, A., Terpiłowski, K., Martín-Lara, M.A., 2023. On the use of plastic precursors for preparation of activated carbons and their evaluation in CO_2 capture for biogas upgrading: a review. Waste Manag. 161, 116–141. https://doi.org/10.1016/J.WASMAN.2023.02.022.

Pimentel, C.H., Díaz-Fernández, L., Gómez-Díaz, D., Freire, M.S., González-Álvarez, J., 2023. Separation of CO_2 using biochar and KOH and $ZnCl_2$ activated carbons derived from pine sawdust. J. Environ. Chem. Eng. 11, 111378 https://doi.org/10.1016/J.JECE.2023.111378.

Pu, Q., Zou, J., Wang, J., Lu, S., Ning, P., Huang, L., Wang, Q., 2021. Systematic study of dynamic CO_2 adsorption on activated carbons derived from different biomass. J. Alloy. Compd. 887, 161406 https://doi.org/10.1016/J.JALLCOM.2021.161406.

Quan, C., Wang, H., Jia, X., Gao, N., 2021. Effect of carbonization temperature on CO_2 adsorption behavior of activated coal char. J. Energy Inst. 97, 92–99. https://doi.org/10.1016/J.JOEI.2021.04.003.

Ramírez-Valencia, L.D., Bailón-García, E., Moral-Rodríguez, A.I., Carrasco-Marín, F., Pérez-Cadenas, A.F., 2023. Carbon Gels–Green Graphene Composites as Metal-Free Bifunctional Electro-Fenton Catalysts. Gels 9, 665. https://doi.org/10.3390/GELS9080665.

Ramos, P.B., Ponce, M.F., Jerez, F., Barreto, G.P., Bavio, M.A., 2022. Assessment of industrial waste for adsorption and capture of CO_2: Dynamic and static capture system. J. Environ. Chem. Eng. 10, 107521 https://doi.org/10.1016/J.JECE.2022.107521.

Rasi, S., Veijanen, A., Rintala, J., 2007. Trace compounds of biogas from different biogas production plants. Energy 32, 1375–1380. https://doi.org/10.1016/J.ENERGY.2006.10.018.

Raymundo-Piñero, E., Azaïs, P., Cacciaguerra, T., Cazorla-Amorós, D., Linares-Solano, A., Béguin, F., 2005. KOH and NaOH activation mechanisms of multiwalled carbon nanotubes with different structural organisation. Carbon N. Y 43, 786–795. https://doi.org/10.1016/J.CARBON.2004.11.005.

Roy, P., Dias, G., 2017. Prospects for pyrolysis technologies in the bioenergy sector: A review. Renew. Sustain. Energy Rev. 77, 59–69. https://doi.org/10.1016/J.RSER.2017.03.136.

Saleh, T.A., 2022. Adsorption technology and surface science. Interface Sci. Technol. 34 39–64. https://doi.org/10.1016/B978-0-12-849876-7.00006-3.

Saptoadi, H., Rohmat, T.A., Sutoyo, 2016. Combustion of char from plastic wastes pyrolysis. AIP Conf Proc 1737. https://doi.org/10.1063/1.4949286/884789.

Sevilla, M., Díez, N., Fuertes, A.B., 2021. Toward More Sustainable Chemical Activation Strategies for the Production of Porous Carbons. ChemSusChem 14, 94–117. https://doi.org/10.1002/CSSC.202001838.

Sevilla, M., Fuertes, A.B., 2016. A Green Approach to High-Performance Supercapacitor Electrodes: The Chemical Activation of Hydrochar with Potassium Bicarbonate. ChemSusChem 9, 1880–1888. https://doi.org/10.1002/CSSC.201600426.

Sevilla, M., Parra, J.B., Fuertes, A.B., 2013. Assessment of the role of micropore size and N-doping in CO_2 capture by porous carbons. ACS Appl. Mater. Interfaces 5, 6360–6368. https://doi.org/10.1021/AM401423B.

Shah, H.H., Amin, M., Iqbal, A., Nadeem, I., Kalin, M., Soomar, A.M., Galal, A.M., 2023. A review on gasification and pyrolysis of waste plastics. Front Chem. 10, 960894 https://doi.org/10.3389/FCHEM.2022.960894.

Singh, J., Bhunia, H., Basu, S., 2019. Adsorption of CO_2 on KOH activated carbon adsorbents: Effect of different mass ratios. J. Environ. Manag. 250, 109457 https://doi.org/10.1016/J.JENVMAN.2019.109457.

Singh, G., Maria Ruban, A., Geng, X., Vinu, A., 2023. Recognizing the potential of K-salts, apart from KOH, for generating porous carbons using chemical activation. Chem. Eng. J. 451, 139045 https://doi.org/10.1016/J.CEJ.2022.139045.

Sitthikhankaew, R., Predapitakkun, S., Kiattikomol, R., Pumhiran, S., Assabumrungrat, S., Laosiripojana, N., 2011. Comparative Study of Hydrogen Sulfide Adsorption by using Alkaline Impregnated Activated Carbons for Hot Fuel Gas Purification. Energy Procedia 9, 15–24. https://doi.org/10.1016/J.EGYPRO.2011.09.003.

Soffian, M.S., Abdul Halim, F.Z., Aziz, F., A . Rahman, M., Mohamed Amin, M.A., Awang Chee, D.N., 2022. Carbon-based material derived from biomass waste for wastewater treatment. Environ. Adv. 9, 100259 https://doi.org/10.1016/J.ENVADV.2022.100259.

Solís, R.R., González, M. del C., Blázquez, G., Calero, M., Martín-Lara, M.Á., 2023. Activated char from the co-pyrolysis of polystyrene and olive stone mixtures for the adsorption of CO_2. J. Environ. Chem. Eng. 11, 111370 https://doi.org/10.1016/J.JECE.2023.111370.

Tan, Y.L., Islam, M.A., Asif, M., Hameed, B.H., 2014. Adsorption of carbon dioxide by sodium hydroxide-modified granular coconut shell activated carbon in a fixed bed. Energy 77, 926–931. https://doi.org/10.1016/J.ENERGY.2014.09.079.

Tang, S., Sun, P., Ma, S., Jin, W., Zhao, Y., 2023. The interfacial behaviors of different arsenic species on polyethylene mulching film microplastics: Roles of the plastic additives. J. Hazard Mater. 442, 130037 https://doi.org/10.1016/J.JHAZMAT.2022.130037.

Teng, H., Lin, Y.C., Hsu, L.Y., 2011. Production of Activated Carbons from Pyrolysis of Waste Tires Impregnated with Potassium Hydroxide. J. Air Waste Manag. Assoc. 50, 1940–1946. https://doi.org/10.1080/10473289.2000.10464221.

Toprak, A., Hazer, B., 2023. Synthesis of microporous hollow spherical polystyrene carbons for the highly efficient CO2 adsorption and selectivity. J. Ind. Eng. Chem. 127, 295–302. https://doi.org/10.1016/J.JIEC.2023.07.015.

Varghese, S.M., Chowdhury, A.R., Arnepalli, D.N., Ranga Rao, G., 2023. Delineating the effects of pore structure and N-doping on CO_2 adsorption using coco peat derived carbon. Carbon Trends 10, 100250. https://doi.org/10.1016/J.CARTRE.2023.100250.

Wang, X., Chen, L., Guo, Q., 2015. Development of hybrid amine-functionalized MCM-41 sorbents for CO_2 capture. Chem. Eng. J. 260, 573–581. https://doi.org/10.1016/J.CEJ.2014.08.107.

Wang, H., Jahandar Lashaki, M., Fayaz, M., Hashisho, Z., Philips, J.H., Anderson, J.E., Nichols, M., 2012. Adsorption and desorption of mixtures of organic vapors on beaded activated carbon. Environ. Sci. Technol. 46, 8341–8350. https://doi.org/10.1021/ES3013062.

Wang, J., Yuan, X., Deng, S., Zeng, X., Yu, Z., Li, S., Li, K., 2020. Waste polyethylene terephthalate (PET) plastics-derived activated carbon for CO_2 capture: a route to a closed carbon loop. Green. Chem. 22, 6836–6845. https://doi.org/10.1039/D0GC01613F.

Wang, X., Zeng, W., Kong, X., Xin, C., Dong, Y., Hu, X., Guo, Q., 2022. Development of Low-Cost Porous Carbons through Alkali Activation of Crop Waste for CO_2 Capture. ACS Omega 7, 46992–47001. https://doi.org/10.1021/ACSOMEGA.2C06109.

Wijesekara, D.A., Sargent, P., Ennis, C.J., Hughes, D., 2021. Prospects of using chars derived from mixed post waste plastic pyrolysis in civil engineering applications. J. Clean. Prod. 317, 128212 https://doi.org/10.1016/J.JCLEPRO.2021.128212.

Yu, S., Bo, J., Fengjuan, L., 2019. Competitive adsorption of $CO_2/N_2/CH_4$ onto coal vitrinite macromolecular: Effects of electrostatic interactions and oxygen functionalities. Fuel 235, 23–38. https://doi.org/10.1016/J.FUEL.2018.07.087.

Yuan, X., Lee, J.G., Yun, H., Deng, S., Kim, Y.J., Lee, J.E., Kwak, S.K., Lee, K.B., 2020. Solving two environmental issues simultaneously: Waste polyethylene terephthalate plastic bottle-derived microporous carbons for capturing CO_2. Chem. Eng. J. 397, 125350 https://doi.org/10.1016/J.CEJ.2020.125350.

Zaitan, H., Manero, M.H., Valdés, H., 2016. Application of high silica zeolite ZSM-5 in a hybrid treatment process based on sequential adsorption and ozonation for VOCs elimination. J. Environ. Sci. 41, 59–68. https://doi.org/10.1016/J.JES.2015.05.021.

Zhang, S., Jia, Xiangdong, Wang, X., Chen, J., Cheng, C., Jia, Xichuan, Hu, H., 2024. Using the Conditional Process Analysis Model to Characterize the Evolution of Carbon Structure in Taxodium ascendens Biochar with Varied Pyrolysis Temperature and Holding Time. Plants 13, 460. https://doi.org/10.3390/PLANTS13030460.

Zhang, K., Sun, J., E, L., Ma, C., Luo, S., Wu, Z., Li, W., Liu, S., 2022. Effects of the Pore Structure of Commercial Activated Carbon on the Electrochemical Performance of Supercapacitors. J. Energy Storage 45, 103457. https://doi.org/10.1016/J.EST.2021.103457.